Multimodal 3D computer planning system for the implantation of stereotactic electrodes in refractory epilepsy

Alfredo Higueras-Esteban

TESI DOCTORAL UPF / YEAR 2021

Directors de la tesi

Dr. Miguel Ángel González Ballester [1,2]
Dr. Luis Serra [3]

[1] Universitat Pompeu Fabra

[2] ICREA, Barcelona, Spain

[3] Galgo Medical S.L., Barcelona, Spain.

DEPARTMENT OF INFORMATION AND COMMUNICATION TECHNOLOGIES

upf. Universitat
Pompeu Fabra
Barcelona

To the memory of those who could not stay,
and to those who are today among us.

Acknowledgments

Abstract

Neurosurgery is evolving towards the use of minimally invasive procedures. In this dissertation, we present several tools designed to fulfill the multimodal and multidisciplinary requirements of Stereoencephalography (SEEG) and epilepsy surgery. The resulting planning platform, named SYLVIUS, provides a digitalized workflow intended to facilitate clinical decision-making which has been used in Hospital del Mar, Barcelona for the evaluation of nineteen SEEG implantations. The platform allows for 3D-stereo visualization and interaction with head-tracking capabilities, providing novel interaction tools for the analysis of vascular and tractography data. Also, we present a clinical study of the risks and benefits of using digital subtraction angiography (DSA) performed with SYLVIUS. Finally, we describe two interactive trajectory planning tools, one designed to early signal the presence of vascular structures near a trajectory, and another one to find avascular alternative paths to a given potentially dangerous one maximizing adherence to either the entry, the target, or the insertion angle of the initial trajectory.

Keywords: Epilepsy surgery, Stereoelectroencephalography (SEEG), Diffusion-weighted imaging (DWI), Angiography, Surgical workflow, Multimodal, Multidisciplinary, Stereotactic neurosurgery.

Resumen

La neurocirugía está evolucionando hacia el uso de procedimientos mínimamente invasivos. En esta disertación, presentamos varias herramientas diseñadas para cumplir con los requisitos multimodales y multidisciplinarios de la estereoencefalografía (SEEG) y la cirugía de epilepsia. La plataforma de planificación resultante, denominada SYLVIUS, proporciona un flujo de trabajo digitalizado destinado a facilitar la toma de decisiones clínicas que se ha utilizado en el Hospital del Mar de Barcelona para la evaluación de diecinueve implantaciones de SEEG. La plataforma permite la visualización e interacción en estéreo 3D con capacidades de seguimiento de la cabeza, proporcionando nuevas herramientas de interacción para el análisis de datos vasculares y de tractografía. Además, presentamos un estudio clínico de los riesgos y beneficios del uso de la angiografía por sustracción digital realizada con SYLVIUS. Finalmente, describimos dos herramientas interactivas de planificación de trayectorias, una diseñada para señalar tempranamente la presencia de estructuras vasculares cerca de una trayectoria, y otra para encontrar rutas alternativas avasculares a una trayectoria potencialmente peligrosa, maximizando la adherencia a la entrada, el objetivo o el ángulo de inserción.

Palabras clave: Cirugía de epilepsia, estereoelectroencefalografía (SEEG), Imagen ponderada por difusión (DWI), Angiografía, Flujo de trabajo quirúrgico, Multimodal, Multidisciplinar, Neurocirugía estereotáctica.

Contents

Acronyms and abbreviations

CAP   Computer-assisted planning

DRE   Drug-resistant epilepsy

AED   Anti-epileptic drugs

EEG   Electroencephalography

SEEG   Stereoelectroencephalography

LITT   Laser interstitial thermal therapy

HIFU   High-intensity focused ultrasound

MRI   Magnetic resonance imaging

PET   Positron emission tomography

CT   Computerized tomography

ILAE   International League Against Epilepsy

GPU   Graphics processing unit

MIP   Maximum intensity projection

List of figures

List of tables

1 INTRODUCTION

"The operating is the easy part, you know,' he said. 'By my age you realize that the difficulties are all to do with the decision-making."
— **Henry Marsh. Neurosurgeon.**
Do no harm: stories of life, death, and brain surgery

Neurosurgery is evolving from open surgery into minimally invasive approaches [1]. These minimally invasive approaches provide significant benefits for the patients, who recover earlier, suffer less collateral damage, and incur less risk of infection allowing them to return to their normal lives earlier [2]. This kind of procedure also saves costs, affords access to this treatment to more patients due to shorter hospital stays, compared with open surgery [3].

Stereotactic neurosurgery has been defined as "the technique for locating targets of surgical interest within the brain relative to an external frame of reference" [4]. Some of these procedures include the insertion of rectilinear devices like electrodes, laser probes, or biopsy needles [5], which can be implanted with either stereotactic frames, neuro-navigators, or frameless systems, and more recently, neurosurgical robots [6]. Other stereotactic procedures reach the target without incisions, like HIFU [7] or radiosurgery [8, 9].

Stereotactic procedures require neurosurgeons to plan the intervention [10]. In stereotactic neurosurgery, in contrast to open neurosurgery, there is no direct view on the surgical field, and all decision-making regarding the insertion point, angle, and depth must be done before the intervention by carefully inspecting preoperative data.

Important advances in medical imaging have made available precise information about the anatomy of the patient obtained using different 3D acquisition techniques which take advantage of the physical properties of the human body [6]. Nevertheless, not all information used for surgical

planning is 3D. Important examples of non-3D datasets are electrical observations and patient symptomatology [11].

Furthermore, decision-making in stereotactic neurosurgery requires close collaboration between multiple medical specialties [12], like neuroradiology, neurology, nuclear medicine, neuropsychology, and neurosurgery.

The disciplines involved carefully examine preoperative data to come up with the most effective and safest trajectories. They do so by using a variety of software and hardware that form what is referred to as the surgical planning platform. Some of these surgical planning platforms are provided by the implantation hardware (e.g., the robot) manufacturer, others are sold separately by dedicated medical companies, and some are developed in the context of academic research.

1.1   Refractory epilepsy

Epilepsy is a term that evolved from ancient Greek, and which means to seize or possess. Some ancient texts seem to refer to epilepsy, many times assigning it a magical or mystical nature. Within the Hippocratic Corpus (a collection of Greek classical medicine) it is stated clearly that epilepsy has a natural cause and that it is no more sacred or mystical than any other disease, being one of the oldest exponents of rational or scientific medicine. The discovery of the electroencephalogram (EEG) by a German psychiatrist in 1924 cleared the way to the present electrical understanding of epileptic seizures.

A modern definition of epilepsy could be "a disorder of the brain characterized by an enduring predisposition to generate epileptic seizures" [13]. The accumulated knowledge has allowed concluding that it is not a single syndrome but a family of them, which is sometimes referred to as *the epilepsies*. The International League Against Epilepsy (ILAE) states that possible causes might be structural, genetic, infectious, metabolic, immune, or unknown causes [14]. ILAE also classifies epilepsy as either "Focal", "Generalized", "Combined Generalized and Focal" and "Unknown".

The published prevalence of epilepsy ranges from 4 to 10 per 1000 in developed countries [15]. For most patients, it is a chronic condition, and they require treatment to stop seizures. The most common treatment is the use of antiepileptic drugs (AED). Initial AED provided limited seizure control and strong side effects [16]. Modern antiepileptic drugs like

Vigabatrin and Gabapentin are designed to selectively affect synapses, mostly by affecting the GABA neurotransmitter [17].

It is estimated that around 30%-40% of patients do not respond to antiepileptic drugs [15]. Those cases are referred to as refractory epilepsy, or drug-resistant epilepsy (DRE). For those, epilepsy surgery might be the right treatment.

Refractory epilepsy surgical treatment includes two important steps. First, it is necessary to delimit if there is a single area responsible for seizure onset. For that, many non-invasive diagnostic tools may be employed. When non-invasive techniques fail to locate the EZ, invasive diagnostic techniques such as stereotactic electroencephalography (SEEG) can be used [18], which consists on the placement of several rectilinear depth electrodes that are used to measure electric fields inside the brain. After that, the second step of epilepsy surgery is the resection or disconnection of that area. That can be performed with several techniques, and some of them also fall under the category of stereotactic neurosurgery, like laser interstitial thermal therapy (LITT).

1.2 Aims and objectives

1.2.1 Aims

There is increasing clinical demand for improvements in surgical planning platforms to increase patient safety, maximize treatment outcomes and generate better decision-making processes involving several specialties. This project seeks to develop advanced surgical planning tools for stereotactic neurosurgery, and in particular for SEEG, to fit that clinical demand. The research will be conducted after performing a software architecture analysis, creating a digitalized workflow with specific tools for the stereotactic treatment of epilepsy surgery, providing means to carry out the clinical evaluation of different vascular imaging modalities, and delivering novel tools for trajectory assessment and replanning.

1.2.2 Objectives

The objectives for this thesis are:

1. Examine the literature for surgical platforms designed for the implantation of SEEG electrodes.

2. Investigate prior work on computer-assisted trajectory planning in SEEG.

3. Generate a digitalized workflow for multimodal and multidisciplinary epilepsy surgery planning.

4. Develop a post-operative Computer Tomography segmentation procedure to extract individual electrode contacts.

5. Create a three-dimensional representation of measured electrical data read from electrophysiological files.

6. Develop advanced DTI filtering with post-operatory CT scan to isolate tracts relevant to the clinical routine based on the final position of the electrodes.

7. Design an assisted or automated trajectory planning system for SEEG implantations.

8. Evaluate the use of different imaging modalities for SEEG electrode implantation.

1.3 Context

The current dissertation has been possible thanks to the collaboration of three main institutions, each one of them providing its unique perspective on research and a different set of resources. First, the Hospital del Mar/IMIM (Barcelona, Spain), a reference hospital specialized in the treatment of complex refractory epilepsy patients with a skilled team of individuals and excellent robotic and neurosurgical planning equipment has exposed some of the unmet needs of modern neurosurgery. Second, the Universitat Pompeu Fabra, a young and vibrant public university based in Barcelona, ranked 152nd this year on the Times Higher Education World University Rankings, provides the rigor of how proper research should be conducted. Finally, Galgo Medical S.L., (Barcelona, Spain), a thoroughly modern company provides experience in creating medical products.

Figure 1.1 Institutional context

The work presented is part of the SYLVIUS project, which has been funded by the "Fundació la Caixa" with the grant "Convenio Generalitat de Catalunya".
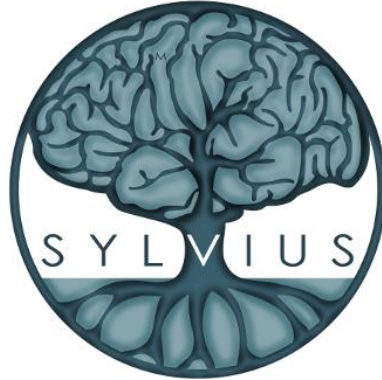
Figure 1.2 SYLVIUS project logo

1.4 Thesis outline and contributions

This work is devoted to enhancing current surgical planning solutions. The main contribution of this thesis is the development of the SYLVIUS planning platform. This work has led to three research manuscripts covering the areas of software architecture, clinical research, and novel algorithms for automated trajectory planning. Furthermore, a patent has been filed, both in Europe and the USA, for the automated trajectory planning method.

In this thesis we first present work related to the general design of a platform for SEEG and epilepsy surgery planning, then we focus on its clinical contributions, and then continue with the presentation of an automated trajectory planning tool before presenting the final conclusions.

The contents of this dissertation are structured as follows:

- **Chapter 2** focuses on the design principles behind SYLVIUS, our epilepsy surgery planning platform. It does so from a software architecture perspective and focusing on its multimodal and multidisciplinary requirements. Specific and general tools are described, as well as the hardware used for 3D stereo visualization. This work led to the following journal publication:

  A. Higueras-Esteban, I. Delgado-Martínez, L. Serrano, A. Principe, C.P. Enriquez, M.A. González Ballester, R. Rocamora, G. Conesa, L. Serra,

SYLVIUS: A multimodal and multidisciplinary platform for epilepsy surgery, Computer Methods and Programs in Biomedicine 203 (2021) 106042. https://doi.org/https://doi.org/10.1016/j.cmpb.2021.106042.

- **Chapter 3** focuses on a specific clinical study performed within the SYLVIUS platform. Specifically, it analyses the use of Digital Subtraction Angiography for the planning of SEEG, providing also a comparison with other used imaging modalities. This study was published in:

  I. Delgado-Martínez, L. Serrano, A. Higueras-Esteban, E. Vivas, R. Rocamora, M.A. González Ballester, L. Serra, G. Conesa, On the Use of Digital Subtraction Angiography in Stereoelectroencephalography Surgical Planning to Prevent Collisions with Vessels, World Neurosurgery. 147 (2021) 47–56. https://doi.org/10.1016/j.wneu.2020.11.103.

- **Chapter 4** describes the main algorithmic contribution of this thesis, which falls inside the area of Computer-Aided Planning. Two tools are described, one to assist in the revision of SEEG trajectories and another to find alternative trajectories to an initial one providing different adherence strategies. This work has been submitted to a journal:

  A. Higueras-Esteban, I. Delgado-Martínez, L. Serrano, N. Infante-Santos, A. Narváez-Martínez, A. Principe, R. Rocamora, G. Conesa, L. Serra, M.A. González Ballester, Projection-based collision detection algorithm for Stereoelectroencephalography (SEEG) electrode risk assessment and re-planning, Submitted (2021).

  And an EU and USA patent have been filed for the developed technology:

  *Higueras Esteban A., Serra L., Conesa G., Delgado-Martínez I., González Ballester M.A. Computer implemented method, a system and computer programs for computing simultaneous rectilinear paths using medical images. **US Patent** application no. 16/902912, 16 June 2020*

  *Higueras A., Serra L., Conesa G., Delgado-Martínez I., González Ballester M.A. A computer implemented method, a system and computer programs for computing simultaneous rectilinear paths using medical images. **European Patent** application no. EP19382502, 17 June 2019.*

- **Chapter 5** contains the final conclusions of this thesis and describes the lines for future work.

2 SURGICAL PLANNING PLATFORM

2.1 Introduction

2.1.1 Epilepsy treatment

Around one third of epilepsy patients do not respond to anti-epileptic drugs [15][19] and are potential candidates for epilepsy surgery, a procedure which consists on the removal or disconnection of the epileptogenic zone (EZ). Defining the EZ is a complex issue [20] but some definitions are: "the site of the beginning and of primary organization of the epileptic seizures" [21, 22] or "the minimum amount of cortex that must be resected (inactivated or completely disconnected) to produce seizure freedom"[23].

Thanks to intraoperative neurophysiological monitoring and careful presurgical planning it is possible to safely operate in a variety of areas inside the brain, although sometimes surgery must be discarded (e.g.,., when the EZ cannot be located). Epileptologists usually study the semiology and may use a variety of non-invasive techniques to locate the EZ like electroencephalography (EEG), magnetic resonance imaging (MRI), positron emission tomography (PET), or single-photon emission computed tomography (SPECT)[24].

When non-invasive techniques fail to locate the EZ, invasive diagnostic techniques such as stereotactic electroencephalography (SEEG) can be used. SEEG was developed in the second half of the last century [25] and has since then made great progress alongside 3D multimodal imaging and the use of new surgical devices, in particular robots. Despite these advances, the core methodology remains unaltered, consisting in the stereotactic placement of a

---

number of intracerebral depth electrodes for several days (Gonzalez-Martinez et al. reported 7 days on average [26]), yielding precise electrical recordings of brain activity both during and between seizures.

It is usual for the SEEG planning to start with an initial plan proposed by the epileptologist based on an EZ localization hypothesis to prove or discard the presence of the EZ in several possible locations. This plan is then discussed with the neurosurgeons who can use different systems (frame-based, frameless, and robotic[27]) for the implantation. The next step is usually to introduce the initial epileptology plan into a surgical planning software -many times provided by the stereotactic neurosurgical hardware manufacturer- and refine it to mitigate surgical risks, which may require new imaging modalities. Despite the increasing sophistication of these tools, the planning process still involves manual scrolling through the image planes to find avascular trajectories, which has been described in the literature as an error-prone, inefficient, and time-consuming process [28].

If the EZ is identified, the final step is for the epileptologist to delineate the area of the brain to be removed and for the neurosurgeons to use the most suitable surgical approach to perform the intervention. This could be a craniotomy followed by a resection, laser ablation, or radiofrequency thermocoagulation [29]. Again, precise communication between epileptologists and neurosurgeons is crucial.

Being multidisciplinary, epilepsy surgery may present strong multimodal requirements. Adding to the previously mentioned datasets, modalities like double-contrast Gadolinium MRI (T1-Gd), Angio-CT with bolus injection or digital subtraction angiography (DSA) among others may be used to avoid vasculature, computer tomography (CT) may be used during the intervention for registration with the frame/robot and after electrode implantation for validation, and diffusion-weighted imaging (DWI) and functional magnetic resonance imaging (fMRI) can be of use to locate functional areas to protect and to study EZ connectivity. Neuroscientists sometimes play a support role in processing DWI using tools such as MITK-DI [30], Startrack [31], or MRtrix [32], voxel-based morphometry (VBM)

[33], analyzing fMRI [34], running source localization algorithms [35] or performing segmentation tasks [36], providing even more datasets.

The presented work describes a new system aiming to provide a patient-centered application structure that allows for storing and sharing different stages of SEEG and epilepsy surgery. It describes both a workflow, as well as several generic and specific tools.

2.1.2 Related work

The Ospedale Niguarda group [37, 38] has extensive experience in the surgical treatment of epilepsy and the use and development of several software tools for it. Their workflow introduced the use of DSA for the multimodal evaluation of SEEG implantation [39], where DSA constitutes the reference space to which all datasets are registered. The group presented a 3D Slicer module to automatically define SEEG trajectories given a target point and possible entry points [40, 41]. In [42] a tool is presented in which, for each electrode, a maximum intensity projection (MIP) image is obtained by projecting a portion of one centimeter of the vessel volume on a plane perpendicular to the electrode trajectory. Yet another 3D Slicer module was presented in [43] dedicated to assisting the clinical team in the post-implant stage. 3D Slicer input is untagged, and the tools are usually configured selecting datasets by name from drop-down lists.

Another relevant platform is EpiNav [44], which has a dedicated user interface specially designed for epilepsy, and it has been used as a clinical decision support tool[45]. It allows for multimodal image registration[10], 3D mesh model generation and visualization, and manual and automated electrode planning among other features. Images are imported into the case through drag and drop. Data import is again untagged, and tools require the user to identify the input datasets by name from all the imported ones. In [46] a pipeline for the creation of multimodal cases is presented which is an attempt to provide a comprehensive workflow. It describes a fixed image integration scheme, where all datasets are registered to a T1-weighted image. EpiNav also provides a risk profile visualization along the trajectory designed to easily inform the surgeon of the vicinity of

risks along a given trajectory [47]. EpiNav can also import Freesurfer segmentations.

IBIS [48, 49] is a neuronavigation system that incorporates an automatic planner for SEEG with the novelty that it attempts to maximize intracranial EEG recording from the volume of interest and its surroundings. It is a system with advanced Augmented Reality (AR) and registration capabilities. It organizes datasets in a hierarchical structure, where each node contains a transform (i.e.: a mathematical operation that allows modifying the medical dataset location in 3D space), and it is concatenated with the transform of its parent nodes, which prevents image resampling upon registration. In [50] they use tubes -instead of lines- to represent electrode trajectories, a feature that can also be found in commercial systems to define a security zone surrounding the electrode. To the best of our knowledge, this software can be used for SEEG interventions, but no concept of workflow is built into the platform.

A procedure that shares some similarities with SEEG is Deep Brain Stimulation (DBS), where software solutions like Cirerone [51] and CranialVault [52] have been developed to address the issue of workflow and data transfer among the various stages. In [53] a tool is presented for the optimization of DBS electrodes based on geometric constraints. The tool focuses on the risk computation of insertion points (or entry points) for a given target point. A visualization of the risks associated with each entry point is presented, designed to facilitate decision making. Despite similarities with SEEG, in DBS the target point is fixed (is the point to be stimulated) whereas in SEEG both the entry and the target point can be moved, and risk visualization projected on the cortex does not seem suitable for displaying the entire set of possible trajectories.

AR and VR have been proposed to aid both at the pre-operative and intra-operative [54] stages of the planning and insertion of rectilinear trajectories inside the brain. The Dextroscope [55] is a VR environment that provides a 3D representation of the patient data based on multimodal volume rendering. The user can manipulate the 3D rendered image with two handheld controllers, allowing for intuitive exploration of the surgical field as well as three-dimensional planning of rectilinear trajectories. In [56] an AR planning system

was presented which only presents blood vessels and critical structures in the vicinity of the planned trajectory allowing the user to concentrate only on the relevant structures. Our work aims to integrate this functionality in those places where it may be required in the context of epilepsy surgery planning.

In conclusion, epilepsy surgery is a complex procedure with strong multimodality requirements, but there are also multidisciplinary concerns (i.e.: fluid communication across the different specialties involved in the procedure), which have to our knowledge not yet been fully addressed. Furthermore, we also aim to simplify the currently available user interfaces and interactions required.

2.1.3 Design principles and main technical contributions

SYLVIUS is a platform that integrates different tools along the epilepsy surgery workflow, and which could be used in a clinical environment. Its workflow is defined by the different SEEG electrodes stages and the final resection: starting from a preliminary plan, the initial surgical plan, a reviewed plan, the executed surgical plan (which can be modified in the operating room), the final postoperative segmented SEEG electrodes and the resection plan. Although the workflow is particularly designed to the way epilepsy surgery is performed in our institution, we believe its general principles can be applied to different implementations of the procedure by modifying small parts of the application. To the best of our knowledge, no other tool has been presented which can represent so many steps of the epilepsy surgery workflow.

For the implementation, we have tried to follow these design principles:

- The clinical user must be able to transfer/compare information from different workflow steps without having exposure to matrices or other mathematical constructs.

- Annotate the data upon import and use that information to automatically configure inputs and rendering parameters. Tools become active only if all required inputs are present and co-registered.

- Avoid image degradation upon registration. The negative effects of image interpolation and resampling [57] can be especially relevant in this procedure due to the number of images involved and the multiple registrations required to merge them.

- Allow a flexible order in which the DICOM images are loaded and registered to each other. The registration scheme should not be fixed.

In the graphical user interface (GUI) domain, a draggable tree diagram with nodes representing the different datasets has been developed to drive registrations, substituting drop-down lists, and giving an idea of the actual registration state.

SYLVIUS also includes several innovations in processing and visualization tools, such as a novel tool to detect DSA vessels inside the security zone, the possibility to filter DWI tractography directly with SEEG electrodes, and the ability to display electrophysiological data directly over the contacts that measure it.

2.2   Description of the system

SYLVIUS is implemented in the C++ programming language and uses a Python wrapper over CMake for project configuration. It uses the wxWidgets library for the Graphical User Interface. VTK, ITK, and MITK are used for visualization, registration, and processing. The overall architecture is plugin based and the structure of the code imposes a clear separation between processing and interaction code. SYLVIUS is only distributed for Windows although its components and its build chain are cross-platform.

When used in a zSpace 300 system (zSpace, Inc., USA), SYLVIUS offers 3D interaction and stereo visualization for working with complex 3D structures (like vessels or white matter tracts, which have geometries that may be hard to visualize in 2D planes and anticipate its shape, unlike, say, a round-shaped tumor). This hardware (depicted in Figure 2.1) is composed of a computer, a stereo screen that emits circularly polarized light, and an integrated infrared

tracking system which allows for pose retrieval (6 degrees of freedom) of polarized glasses and a 3D stylus.
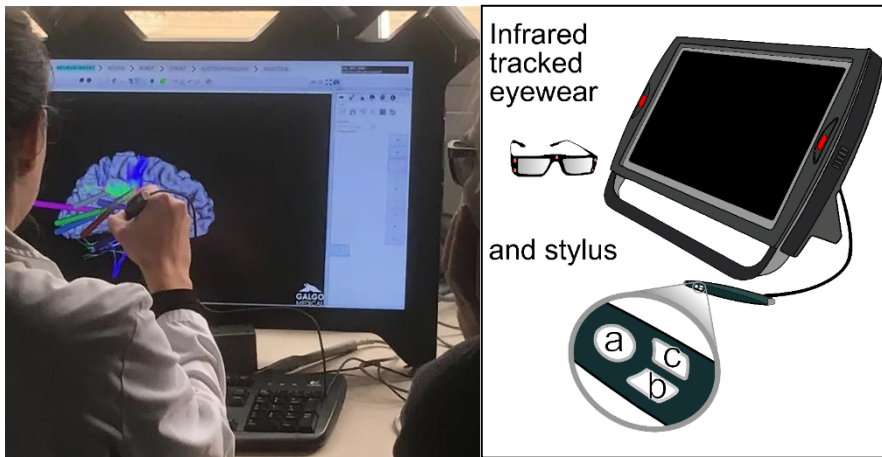
Figure 2.1 zSpace system consisting of a stereo screen with integrated infrared tracking, tracked eyewear, and a tracked 3D stylus with three buttons.

The zSpace glasses movement events are directly connected to a custom subclass of a VTK camera, which renders the scene using two non-symmetric frustums, one for each eye. This technique adds parallax depth cues to the stereo visualization which is intended to reduce the cognitive load associated with the understanding of complex 3D shapes (such as vessels and tractography). Head-tracking is used to provide yet another functionality: the near clipping plane of the aforementioned frustums moves with the tracked glasses allowing the user to clip the scene and examine the internals of a dataset just by moving the head closer to the screen.

2.2.1 Tools common to all disciplines

2.2.1.1 Case Management and Graphical User Interface

Upon start-up, the user can either create a new study or open a previous one. Cases are saved to disk using an internally developed data structure formed by a combination of XML and VTK file formats. A search box allows users to filter cases by patient name. When a new case is created, the software presents itself with most

tools disabled (Figure 2.2) which get activated once their required datasets are imported or become registered.
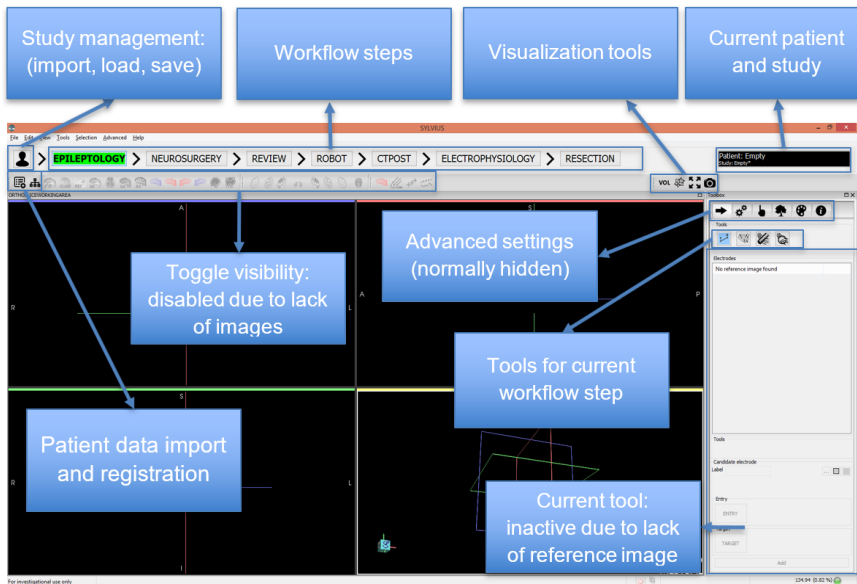
Figure 2.2 General description of SYLVIUS graphical interface

2.2.1.2 Data import

The data import button displays a pop-up window as depicted in Figure 2.3. When a specific modality button is pressed, and a file/folder is selected for import, the volume is loaded annotated as that modality, rendering parameters associated with that modality are applied, relevant processing tools are enabled, the visualization toolbar is updated and the image is marked as present in the import window. This interaction follows our design principle of tagging data upon import.
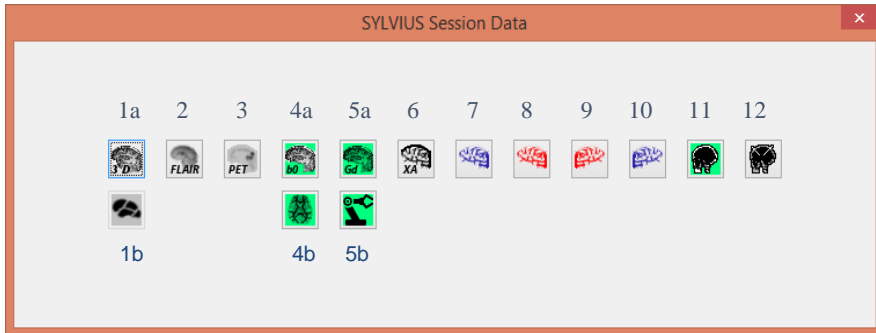
Figure 2.3 Pop-up window for centralized data loading. The datasets already loaded are marked with a green background. (1a) T1-weighted, (1b) Freesurfer, (2) FLAIR, (3) PET, (4a) b0 from diffusion tensor imaging, (4b) Tractography (5a) Double-contrast gadolinium magnetic resonance T1-Gd, (5b) Robot plan, (6-10) X-ray angiographies, one without contrast and four with contrast -left and right, arteriograms and the venograms- XA, (11) Preoperative Computerized Tomography CTpre, (12) Postoperative Computerized tomography CTPost.

Paired datasets, which rely on the presence of other reference data modalities, are presented below their required ones (1b, 4b, and 5b in Figure 2.3) and are disabled if their reference data is not yet imported. For example, tractography (which is generated externally and imported in TrackVis [58] format) requires the presence of the b0 volume which will be later required for registration.

2.2.1.3 Registration GUI and Restrictive Scene Graph

SYLVIUS implements a hierarchical data structure similar to [48]: a scene graph Registration data is stored in relative transform nodes, which modify the pose of their children. This approach avoids unnecessary image degradation [57] upon registration. SYLVIUS uses procedures contained in the MITK framework [59] for registration.

The platform relies on user expertise to choose the pairs of images to register, providing a flexible registration scheme. As in [47], we consider brain shift to be negligible. To prevent mirroring, relative transform nodes are only allowed to contain proper rigid transforms (i.e., matrix determinant must be equal to 1). For dependent datasets (e.g., Freesurfer [36]) the import procedure creates the relative transform node and no further registration is required nor allowed for them.

SYLVIUS provides a simplified scene graph window to manage registrations graphically. It displays only the most relevant datasets, represented with the same icons as the import window and visualization toolbar. A registration procedure is launched by dragging any non-previously registered image icon and dropping it on top of any other volume, as depicted in Figure 2.4. If the registration is validated the view becomes updated and the dragged image and all its children become affected by the computed transformation.
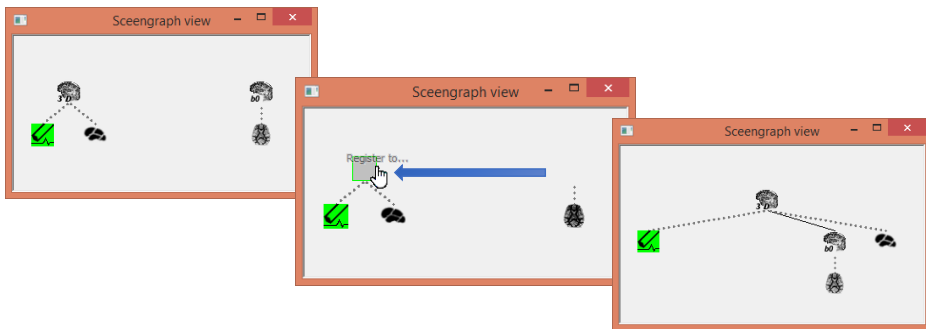
Figure 2.4 Registration GUI . Left: the initial state of the study containing T1 (depicted as 3D), its Freesurfer segmentation and an epileptology electrode plan referenced to it, and an unregistered b0 volume with its dependent tractography. Middle: Launching registration with T1 as fixed image and b0 as moving image by dragging b0 on top T1. Right: after registration session shows all present datasets are registered. Dotted lines represent fixed relationships, and a solid line depicts a relative transform node generated by a registration.

When a dataset is imported, it starts as being disconnected from the rest. To assess that all datasets are registered the user needs only to check that there is a unique tree, as the one depicted in Figure 2.5.
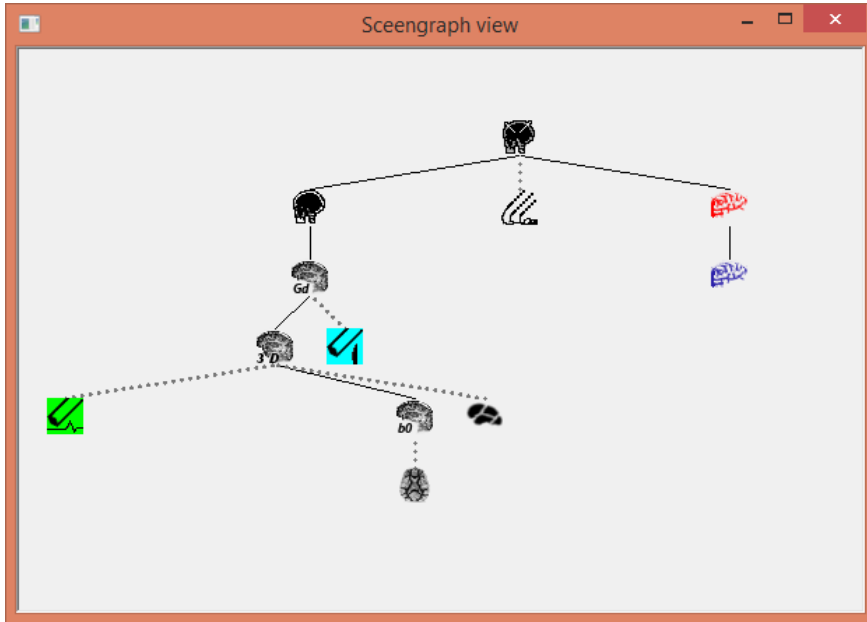
Figure 2.5 Fully registered case, containing several volumes (CTpost, CTpre, MR2c, T1 with Freesurfer, b0 with tractography and two XA) and 3 electrode sets (epileptology, surgery, and the CTpost segmented one).

2.2.2 SYLVIUS Workflow

The workflow is defined by the following steps:

2.2.2.1 Epileptology

The first step in the workflow is taken by epileptologists to define a preliminary SEEG plan. Importing a T1-weighted image is the only prerequisite to adding electrode trajectories, which are stored as children of the T1-weighted image in the scene graph. At this stage, it is common to import a Freesurfer segmentation or to import a FLAIR and a PET.

A mouse trajectory planning tool (Figure 2.6) provides a multi-render window with either an orthogonal view or a "probe's eye view" -as described in [42]-, both of them with an accompanying 3D view. To aid in multidisciplinarity, the epileptologist can leave comments to the neurosurgeon on a per electrode basis. It is also possible to add, modify and delete trajectories in a single 3D stereo window using the zSpace 3D stylus.
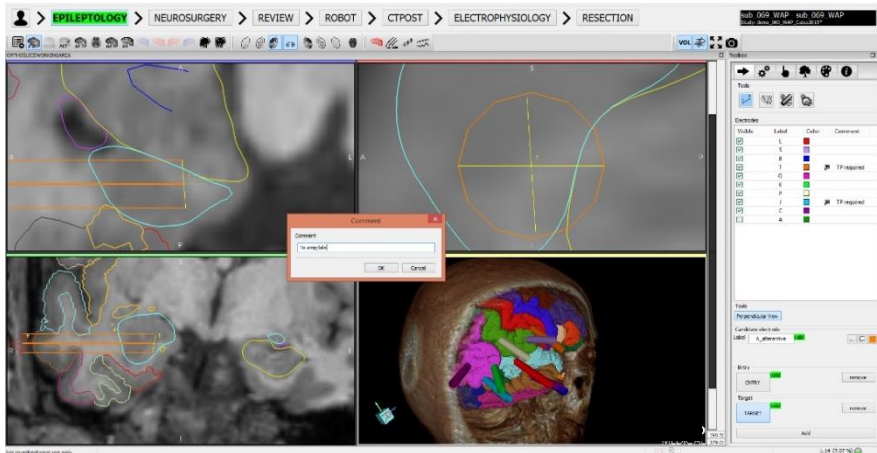
Figure 2.6 Epileptology step : mouse trajectory planning in "probe's eye" view (aligned with the trajectory) plus a 3D view of volume rendered MRT1 and meshes from Freesurfer segmentation. Adding a comment for trajectory inside the amygdala.

2.2.2.2 Neurosurgery

This step is intended for the neurosurgeon to define the first version of the surgical plan based on the previous electrode set. An MR2c image is required to place electrodes. Up to four XA images can be imported to provide greater insight into the vessel structure of the patient.

A "Clone" button allows to precisely transfer the epileptology plan to neurosurgeons, even though they are referred to different coordinate systems (i.e., reference images). The button is enabled when the T1-weighted and MR2c images get co-registered. When clicked, it shows a list of the electrodes from the epileptology electrode set, which can be selected to copy that trajectory in the neurosurgery working area by transparently applying all necessary transformations defined in the scene graph (from T1-weighted space to the MR2c space). Upon cloning, comments show up in a pop-up window.
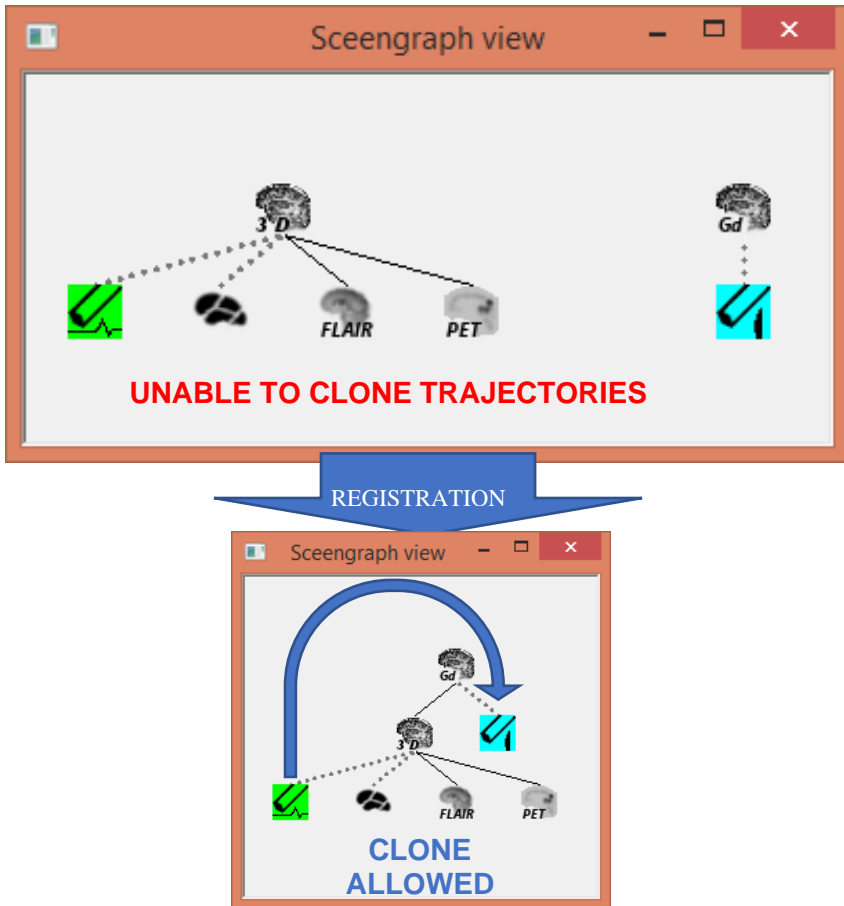
Figure 2.7 Clone activation upon registration. A session with several images loaded before (left) and after (right) registration of the T1 and the MR2c images. Once they are registered the electrodes can be cloned from the Epileptology electrode set (green) into the Neurosurgery electrode set (blue).

Another specific tool of this step is a novel tool to detect collisions of the security zones of the electrodes with vessels briefly described in [60]. This tool is similar to the MIP tool presented by [42] but projects the vessels along the full trajectory. Instead of projecting the maximum intensities, depth is recovered from the z-buffer of the rendering pipeline, which is stored and used for two purposes. When the user clicks on a vessel in the 2D projected image it is used to un-project the 3D point, centering the tri-planar axes on that vessel. Second, depth is mapped to brightness in the projected view, where brighter means closer to entry (Figure 2.8).
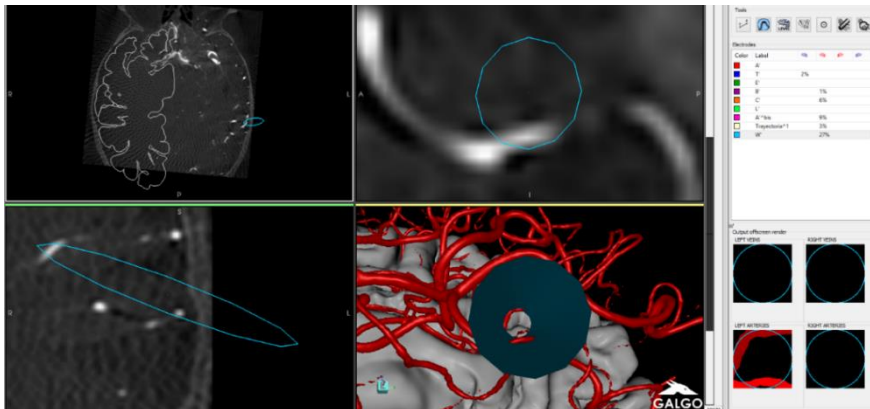
Figure 2.8 Neurosurgery step. Depth Map tool to early detect vessels from up to four XA studies inside the security zone of the planned electrode. For the selected electrode (W') tool indicates 27% of pixels inside the security zone as collisions, which correspond to two distinct vessels at a different depth.

A toolbar button renders the epileptology electrode set (in green wireframe) for a fast visual comparison of the two versions of the plan (Figure 2.9).
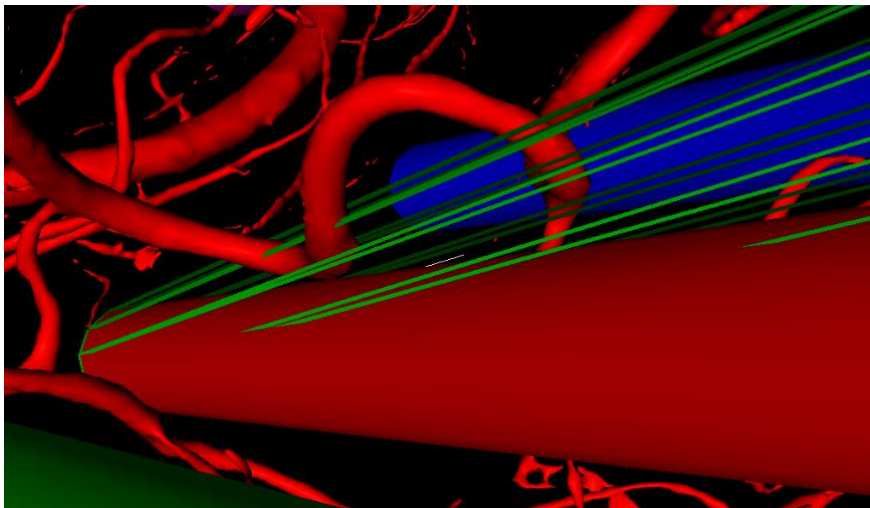
Figure 2.9 Neurosurgery step: comparison of trajectories. The neurosurgery one (solid color) compared with the one defined in the epileptology step (green wireframe). Its entry point has been modified to avoid hitting a vessel detected in the XA image.

2.2.2.3 Review

This step is intended to be used as a consolidation tool in a multidisciplinary meeting between epileptologists and surgeons. The

participants can clone one by one each electrode from the neurosurgery electrode set and check if the modifications performed by the neurosurgeon still measure the desired areas of interest for the epileptologist.

This tab also contains tools to export the electrode set to the intraoperative system in a text file (for our intraoperative prototype), in DICOM format, or navigating to the entry and target point of each electrode in the tri-planar view.

2.2.2.4 Robot

During the electrode implantation, the plan present in the intraoperative system (currently ROSA) can be loaded back into SYLVIUS to keep it synchronized with intraoperative modifications. This also provides enhanced views including images that may not be present in the intraoperative system, as well as advanced tools from SYLVIUS. Furthermore, this also allows us to later analyze intraoperative modifications of the reviewed plan and their causes.

2.2.2.5 CTpost

Once the SEEG electrodes have been implanted, their final position can be obtained from a postoperative CT and managed in the CTpost step. This segmentation obtains the location of each contact (5-18 contacts per electrode). Manually segmenting these contacts is a tedious task, and tools like DEETO [61], Epitools [62], and SEEG Assistant [43] allow for automatic identification of contacts. Our approach to contact segmentation is described in [63], which only requires the CTpost image.
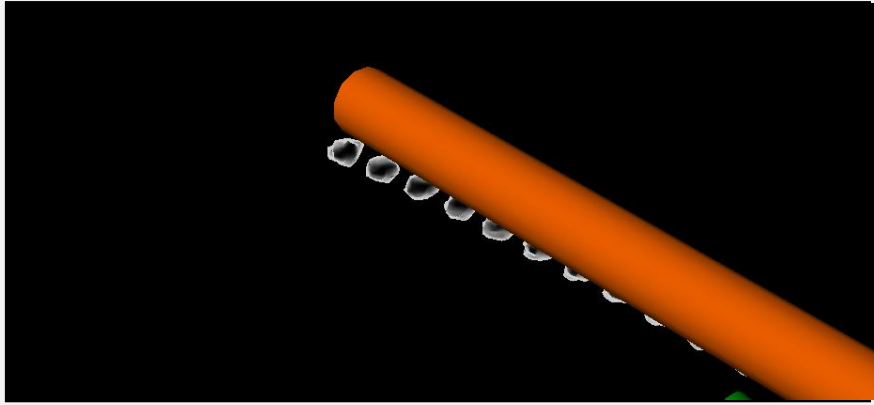
Figure 2.10 Validation of plan with postoperative CT. Upon registration, the user can compare the surgical plan referred to MR2c with the real outcome (using our segmentation method on the postoperative CT).

2.2.2.6 DWI tractography

SYLVIUS itself does not process DWI but it can import a b0 and a whole-brain tractography computed with Startrack [31], Dextroscope[55] in TrackVis [58] format. It is possible to perform freehand 3D stereo tract filtering with a spherical region of interest (ROI) which is positioned with the 3D stylus (Figure 2.11). It is also possible to perform electrode-based tract filtering. The simple mode allows the clinician to filter the tracts that traverse the security zone of one or multiple electrodes simultaneously (AND operation), as depicted in Figure 2.11.
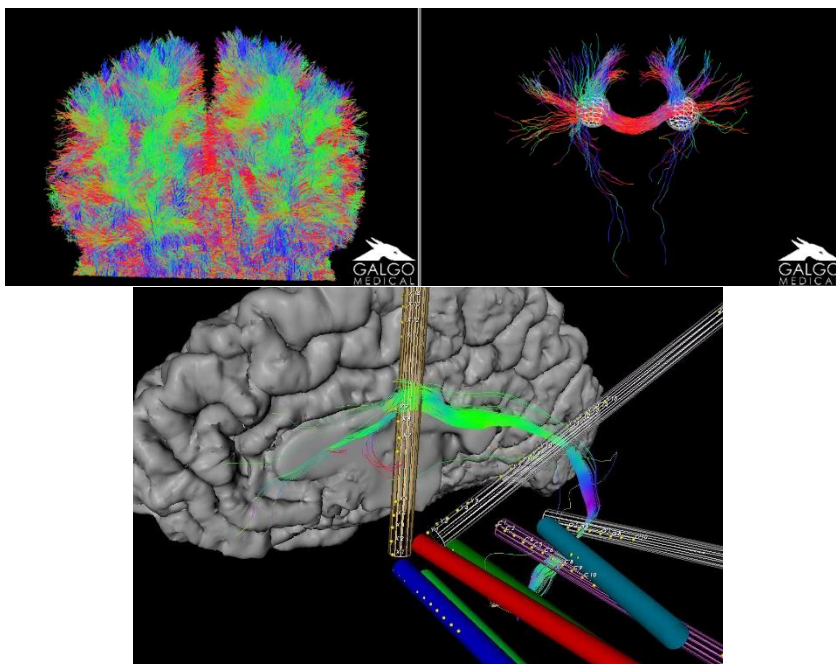
Figure 2.11 DWI tractorgraphy tools. Top: a whole-brain tractography before and after being filtered with two spherical ROI with the AND operation. Bottom: A filtered DWI tractography, displaying only the tracts which traverse the four selected electrodes security zones (in wireframe). The final contact position segmented from CTpost is displayed (yellow spheres).

SYLVIUS can perform a more fine-grained computation to attempt to shed some light on the relation between electrical data measured (SEEG contacts) and the tissue involved in its transmission (tractography), which we have called the SEEG-electrome[64]. This requires a b0 and its corresponding tractography analysis to be registered with the CTpost volume, from which the contact positions are obtained. It then first creates a set of spherical ROIs, either centered on each segmented contact (for unipolar measurements) or placed in the gap between two contacts (for bipolar measurements). Then, it computes all the tracts which traverse at least two contact ROIs at the same time.
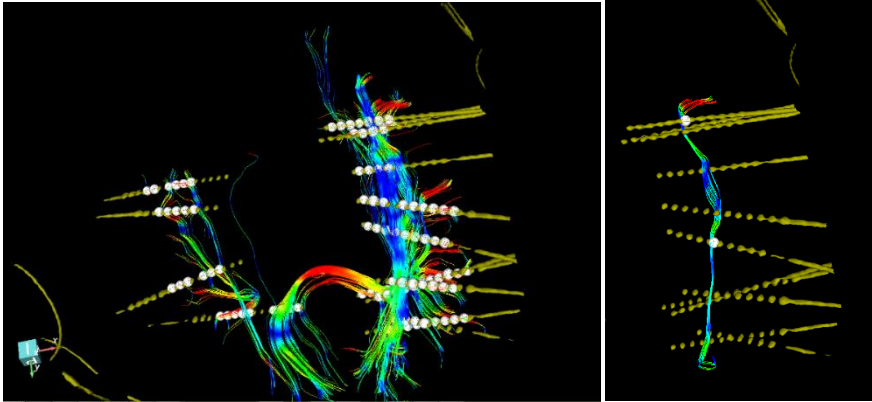
Figure 2.12 SEEG-Electrome computation of a patient with bilateral implantation of SEEG electrodes. Left: aggregated result of the computation. Right: single result from a pair of bipolar spherical ROIs (from SEEG) and the tracts which connect them anatomically (according to the DWI tractography).

2.2.2.7 Electrophysiology

This step provides tools to load and play raw SEEG electrical signals in 3D+t. Data are imported in the European Data Format (EDF) file format, where each signal must have the same name as each contact (i.e., electrode label plus a number). Voltages are normalized and mapped to a color scale used to shade a cylinder of the size of real contact.

Although the presented tool is designed to visualize the raw SEEG readings, it can be used to display the results of electrical data analysis such as correlation analysis or epileptogenicity as in [62].
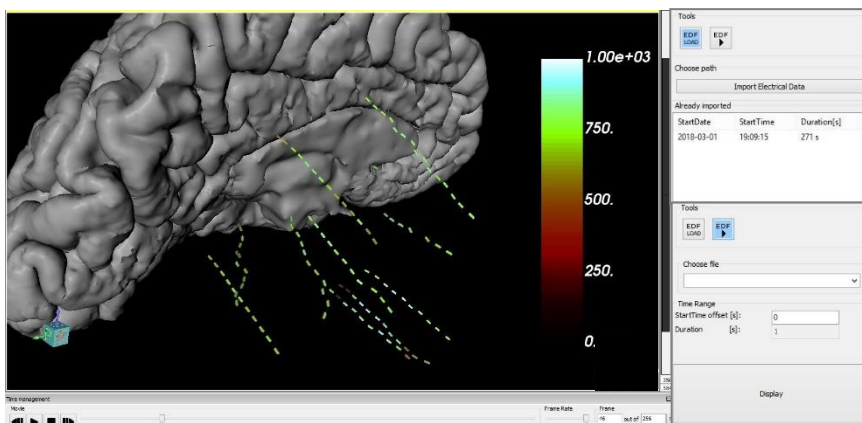
2.2.2.8 Resection

In this last step of the workflow, the epileptologist – based on data collected so far— proposes a resection area of the brain that is revised with the neurosurgeon (Figure 2.14). This step of SYLVIUS allows for a segmented portion of the cortex to be exported in DICOM to the neuronavigation system, in our case the Stealth Station (Medtronic).
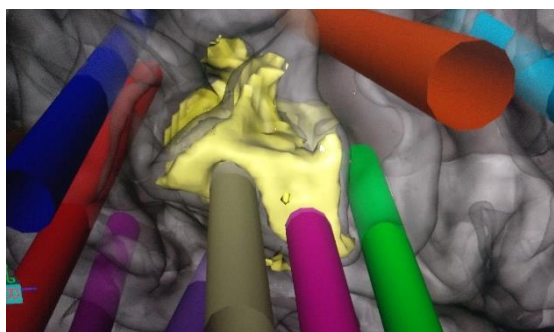
The development of SYLVIUS has accompanied the implantation procedures in Hospital del Mar, Barcelona, Spain (member of EpiCARE, a European Reference Network for rare and complex epilepsies) from 2016 to the present day (58 cases), in progressively higher degrees of involvement. Informed consent was obtained from all patients or their guardians for the data to be used in scientific

27

research and publication (Ethical Committee on clinical investigations Parc de Salut MAR, 2014/5940/I). It has been used to visualize patient data in pre, intra, and postimplantation stages of SEEG, both in 2D and in stereo 3D, and has allowed for the planning and postoperative analysis of SEEG electrodes. As the platform is designed to cover multiple stages of the epilepsy workflow distinct partial results will be presented, all of them integrated by the described architecture.

To evaluate its use as a preimplantation planning tool for SEEG, 19 cases (8 with T1-Gd, and 11 with T1-Gd and DSA) were evaluated. For each patient, modifications from the draft plan following the design provided by the epileptologists to the reviewed surgical plan were analyzed, as well as the reasons given by the neurosurgeons for each change. Reviewed plans were transferred to the ROSA system before the implantation, where the neurosurgeon gave the final approval.

2.3 Results

No complications were reported after the interventions. From the 217 trajectories analyzed within SYLVIUS, 7 were erased, 78 remained unchanged, and the rest had their entry (53), target (10), or both (69) modified. Percentages can be seen in **¡Error! No se encuentra el origen de la referencia.**, both individualized and grouped by the presence or not of DSA. The reasons given for the modifications - aggregated by the presence or not of DSA- are shown in **¡Error! No se encuentra el origen de la referencia.**.
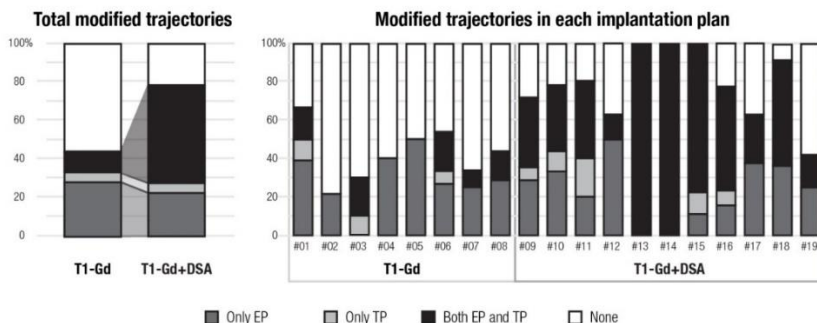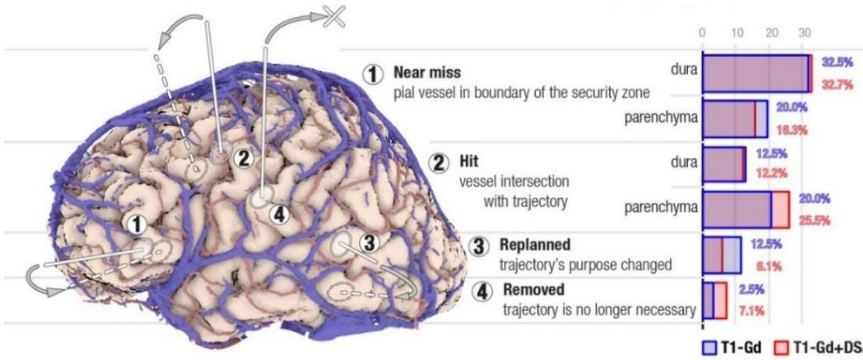
Figure 2.16 Reasons given by the neurosurgeons for the modification of SEEG trajectories by group.

Also in the preoperative stage, the vessel collision detection tool was compared to 2D inspection by a trained neurosurgeon[60], correctly detecting 79.5% of them in under 4 seconds. The only cause for false negatives was low-intensity vessels (below 1500 HU) removed by the threshold segmentation.

In the postimplantation stage, our electrode segmentation tool [63] was used to segment the final position of SEEG electrodes on 24 postoperative CT scans from 18 patients. From a total of 327 electrodes (DIXI Medical) containing 3663 individual contacts, SYLVIUS was able to correctly identify up to 274 with at least 4 contacts, and correctly localize 2422 contacts (66%) in approximately half a minute per case. A comparison of the results of this computation with a manual segmentation can be seen in Figure 2.17.
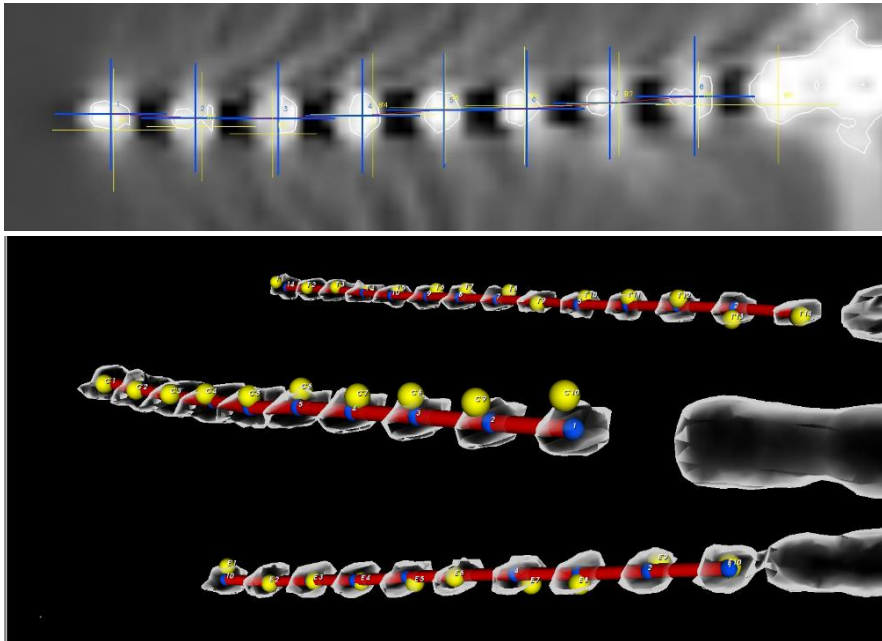
Figure 2.17 Automated contact segmentation. Comparison of the automatic (blue crosses and spheres) and manual (yellow crosses spheres) contact segmentation of SEEG electrodes from a postoperative CT scan.

The SEEG-electrome computation was analyzed [64] in a real clinical case with 163 contacts from 15 electrodes -defining a total of 148 electrical ROIs- and a whole-brain tractography, revealing 147 connections (Figure 2.12) from over $10.000 \binom{148}{2}$ possible pairs. The detected bipolar ROIs sometimes connected ROIS located on the same electrode and sometimes connected distant areas of the brain (e.g., frontal to occipital) from two different electrodes.

2.4   Discussion and future work

One of our guiding principles has been to create tools in which the user requirements are expressed in terms of data availability and validated registrations. Examples of this design are the tractography filtering tools, the functionality to compare and transfer trajectories, or the DSA vessel collision detection tool. The users have been presented with tools that attempt to simplify case construction -such as the data import and the registration widgets- which allow for graphical registration of multimodal datasets. Results show that the

platform has been useful to inspect and modify several trajectories in clinical routine. The higher impact on cases with DSA is explained by the fact that our ROSA robot planning station version is not natively able to load and register DSA datasets.

The impact of zSpace widescreen, volume rendering, and stereo visualization which have been used for the verification of SEEG trajectories has not been quantified. Regarding visualization, the most important lesson learned is that 3D stereo can sometimes provide great insight into the surgical field, but it is a complementary view to the 2D tri-planar, which has its own strengths.

Although the Niguarda group report use of multiple tools, 3D Slicer seems one of its main development platforms. They have used it to visualize two implantation plans versions (manual versus automatic) at the same time using two sets of lines with two different colors. SYLVIUS extends the idea of visualizing different versions of a plan to keep track of the evolution of the plan on time. This feature may be used to visualize/study the adherence of the surgical plan to the epileptology draft plan and to compare the post-operative location of electrodes with the surgical plan -which can also be obtained with SEEG Assistant [43] besides other post-operative functionality-. In our opinion, 3D Slicer is a powerful general-purpose platform that allows for great control over processing, rendering, and data import, but this versatility comes with the cost of a more involved user interface. As data is untagged, tools cannot check if required inputs are present on the study to enable/disable user interaction and whenever a processing tool is used, its inputs must be manually selected by name from drop-down lists. Nevertheless, its generality might be attractive for the most technically capable clinical users. Automatic planning is also available in this system in contrast to SYLVIUS.

EpiNav provides a very interesting tool that gives the user a risk profile along the length of a selected trajectory [47], which we consider complementary to our vessel collision detection tool which looks at the same problem but in the electrode direction. The reason is EpiNav provides only a distance to risky structures, but the direction is lost. In our tool, direction is perceived, but depth is mapped to intensity which is not as precise. Although our tool uses

the GPU to provide fast results, EpiNav has also employed the GPU to compute new trajectories for the user (a review of different computer-assisted planning studies for SEEG can be seen in [45]), which for us will be the subject of future work.

Regarding case construction, fixed registration schemes are described in [46] for EpiNav, where everything is registered to T1-Gd, and in [37] for the Niguarda workflow where everything is registered to DSA. Our architecture offers the possibility to apply both registration strategies, plus a variety of hybrid approaches (e.g., case depicted in Figure 2.5). Choosing one dataset to be always the reference image of the registration is not optimal. For example, DSA may register better to CT, and T1-Gd to T1. Even worse, when the SYLVIUS pipeline starts, none of the above images are usually present (e.g., T1+FreeSurfer+PET). Furthermore, our strategy based on early data annotation and relative transforms allows SYLVIUS users to completely avoid repeating the same transformation for paired data as described in steps 1.4.2.2 to 1.4.2.7 for EpiNav [46]. The example provided is for DWI tractography, which in our architecture happens automatically and transparently to the user. SYLVIUS knows that tractography shares the same space as its reference image (i.e.: b0), and places it correctly upon its registration. Avoiding this interaction can become an advantage for studies like FreeSurfer from which we currently import 107 distinct paired elements (volumes and meshes).

Another benefit of relative transformations, as in IBIS[48], is avoiding image resampling upon registration, preventing unnecessary image degradation[65]. Flat registration schemes with resampling, where everything is registered to a single image, resample N-1 datasets once. For more flexible registration schemes, the worst-case is one dataset being resampled N-1 times. In the case depicted in Figure 2.5, each FreeSurfer volume would have been resampled 4 times. Resampling, besides deteriorating the image[65], prevents processing (e.g., marching cubes) to give identical results before and after registration.

As Freesurfer cannot run on Windows natively, we have provided doctors with a Linux-based Freesurfer virtual machine so that it can be processed in the same physical machine. Sharing a folder between

the host and the virtual machine has shown useful to aid in data transfer.

Our design has a limitation of requiring a T1 for epileptology planning, a T1-Gd for Neurosurgery and review, and a CTpost for extracting the final position of the electrodes. This decision is based on our local workflow and we are aware that centers have distinct pipelines, for example using MR for the postoperative assessment. This can be easily changed and will be configurable in newer versions. Future work will also focus on providing a Frame and a Navigator step to substitute the Robot step in institutions that do not employ a robot for the implantation.

Beyond the initial intended goal of being a clinical tool, SYLVIUS has raised research questions arising from its ability to combine different data modalities. In Figure 2.18 we can see an image that contains a segmented electrode plan, filtered white matter tracts, anatomical information, and electrical readings. We expect that SYLVIUS could find utility in providing a link between the anatomical pathways estimated by the DWI and the SEEG electrical patterns which could be of interest for understanding epileptic seizure propagation, validating DWI tractography algorithms, or measure axonal propagation speed. We believe that this could be the subject of further research and that SYLVIUS and especially its dedicated DWI filtering tools based on electrode and contact positions could aid in the study of such relations.
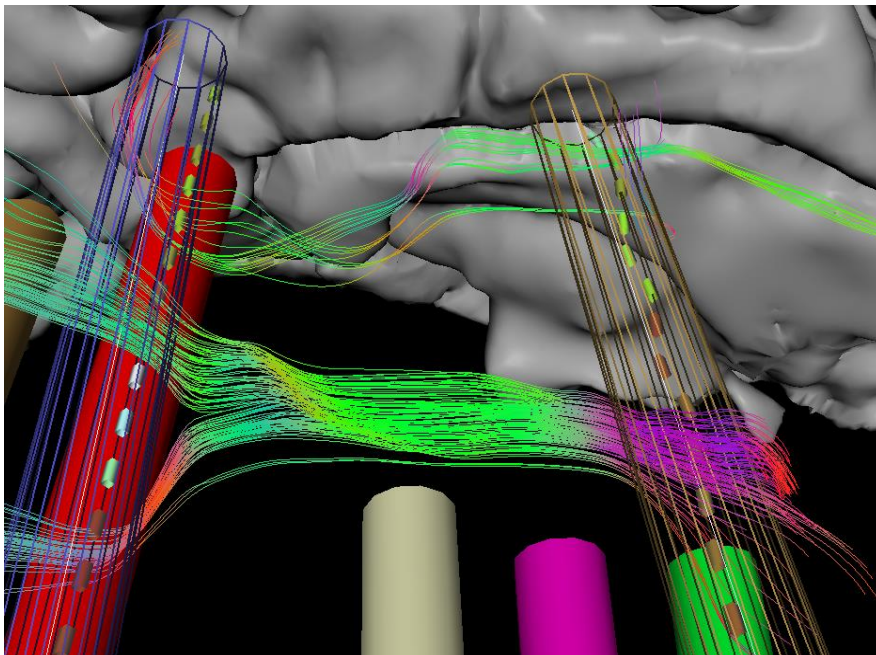
Figure 2.18 Tracts passing through two security zones (in wireframe), a Freesurfer segmentation (back), and electrical data from an EDF file mapped onto segmented contacts (colored cylinders)

We are currently collecting data about other stereotactic uses –DBS for anorexia nervosa and laser interstitial thermal therapy (LiTT) for tumor and epilepsy surgery - and preliminary data suggests that SYLVIUS has been useful in some steps of the procedures (i.e.: exploring DWI tracks to stimulate and vital structures to protect). We will attempt to provide customized workflows for those kinds of interventions in the future.

2.5   Conclusion

In this chapter, we present SYLVIUS, a software platform intended to facilitate and improve the complex workflow of epilepsy surgery providing pre and postoperative tools for electrode implantation and EZ resection. The software uses early data annotation and relative transformations to avoid unnecessary image resampling, automatically configure tools, and simplify the transfer of electrode plans referred to different images. Novel tools for DWI tractography in SEEG have also been described. Lastly, we provide a compact

head-tracking 3D platform to visualize complex anatomical structures such as vessels or segmented white matter tracts.

3   IMPACT ON CLINICAL RESEARCH: Use of DSA in SEEG Surgical Planning

3.1   Introduction

Stereoelectroencephalography (SEEG) is a minimally invasive surgical technique used to determine the location of the epileptogenic network in patients with highly complex focal-resistant epilepsy. [37]. It consists of the insertion of depth electrodes along stereotactic trajectories to obtain electroencephalographic recordings of areas suspected of participating in the generation or propagation of epileptic seizures. This technique avoids the use of a craniotomy, which has considerable risks of complications. [66, 67].

Intracerebral bleeding due to vessel rupture by an electrode is the most frequent complication of SEEG, with an incidence of 1 for every 316 electrodes [68, 69]. To prevent it, the neurosurgeon must carefully plan the electrode trajectories to avoid intersecting vessels. Neuroimaging examinations are fundamental for revealing vascular anatomy during trajectory planning. Gadolinium-enhanced T1-weighted magnetic resonance (T1-Gd) is one of the most established technique in SEEG planning, given its negligible complication rate, availability, and ease [70–73]. Several techniques, like angiographic or venous magnetic resonance imaging (magnetic resonance angiography/magnetic resonance venography), time-of-flight imaging, susceptibility-weighted imaging, or computed tomography angiography, provide superior sensitivity for detecting blood vessels and are commonly used for SEEG planning in addition to T1-Gd [74–77]. The most detailed vascular visualization is achieved with digital

---

subtraction angiography (DSA), permitting distinct visualization of submillimetric vessels [78, 79]. This technique, however, comes with higher complication rates, related to the use of arterial catheterization and high dose of radiation [80]. Although recent publications have stressed the benefits of incorporating DSA into the SEEG workflow [25, 39, 78, 81, 82], the nonnegligible complication rate makes its routine use for SEEG controversial [26, 27, 83, 84].

In this study, we report the contribution of using DSA on the planning of SEEG surgeries in our institution. Three-dimensional reconstruction images from DSA introduced during the revision helped to identify vessels inside the security zone in about two thirds of the trajectories seemingly avascular according to the T1- Gd. The use of CTA did not improve the detection of trajectory-intersecting vessels. DSA information led the neurosurgeon to modify 81.4 ± 4.6 % of the trajectories planned over the T1-Gd sequences. Those modifications only required small shifts of both the entry and target point so that the diagnostic aims were preserved.

On the basis of these findings, we advocate the use of higher resolution vascular imaging techniques, such as DSA, during planning to ensure avoiding vessel-intersecting trajectories.

3.2 Methods

Twenty-two patients undergoing SEEG procedures for drug-resistant epilepsy between 2018 and 2020 at Hospital del Mar (Barcelona, Spain) were selected to participate in this prospective study. All patients consented for the data to be used in scientific research and publication (Ethical Committee on clinical investigations Parc de Salut MAR, 2014/5940/I). All subjects agreed on having an additional preoperative DSA examination for the purpose of this study after being informed about the risks of the procedure.

3.2.1 Imaging equipment and protocols

Magnetic resonance imaging was performed with a 3.0-Tesla unit (Phillips Achieva 3T, Phillips Medical Systems, Eindhoven, The Netherlands). The protocol consisted of a volumetric isometric

sequence of 1-mm thickness (TR=8.5 ms, TE=4.0 ms, and a sampling resolution of 256x256x180 voxels) enhanced with a double 20-mL gadolinium contrast injection. DSA was acquired with a 3-dimensional rotational angiography imaging system (Phillips Allura, Phillips Medical Systems) and reconstructed to a volumetric isometric sequence of 0.32-mm thickness with a sampling resolution of 512x512x512 voxels.

A CTA examination was performed in 6 subjects with the purpose of using it during planning together with the other 2 neuroimaging methods. They were obtained using a 64-row multidetector CT scanner (GE Discovery CT750 HD, General Electric, Fairfield, CT, USA) following the standard protocol of the hospital (120 kV, 100 mAs/ref. and slice thickness of 0.625 mm with administration of a non-ionic iodinated contrast).

The effective dose of DSA was calculated by using the dose-area product (DAP, $Gy \cdot cm^2$) using a dose conversion coefficient [85] of $0.087\ mSv/Gy \cdot cm^2$. For CTA, the effective dose was calculated from the dose-length product (DLP, $mGy \cdot cm$) with a conversion factor [86] of $0.0019\ mS/mGy \cdot cm$.

3.2.2 Planning and revision pipeline

The preoperative planning pipeline began with a diagnostic scheme location proposal for the electrodes made by the epilepsy team based on electrophysiologic, semiologic, and neuroimaging data. This initial proposal does not take into account the patients' vasculature. In the next step, the diagnostic scheme location proposal plan was translated into actual trajectories based on preoperative T1-Gd patient data using the manufacturer planning software for the ROSA robot system (MedTech SA, France) [26, 87]. A 6-mm diameter security zone was set for each trajectory. All the plans were done by the same neurosurgeon (Ms. LS), who had performed >50 implantations with the ROSA system before this study. Special care was taken to place the entry point on the crown of a gyrus and to avoid contrast-enhanced structures from being intersected by the trajectories.
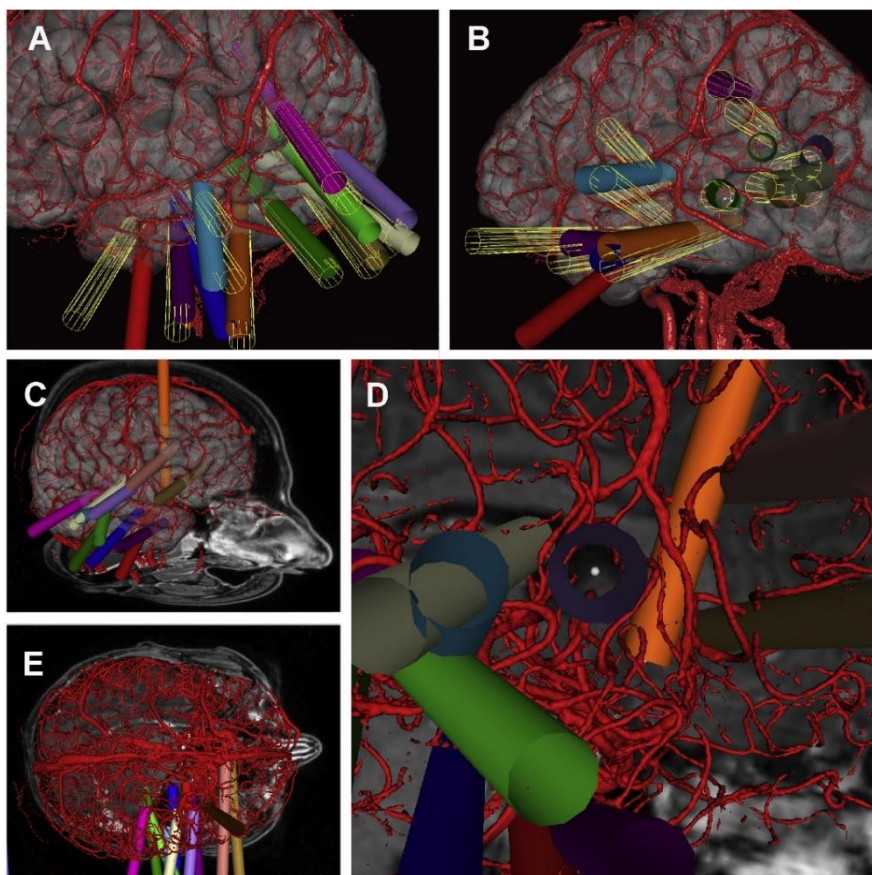
Figure 3.1 Initial and DSA replanned trajectories (A and B) Originally planned trajectories (color-filled tubes) and the corresponding modified plan after revision (yellow wireframe tubes). (C−E) Example screenshots of an avascular trajectory as seen in the SYLVIUS platform.

Since the manufacturer planning software does not allow importing DSA images, the plans were transferred to the multimodal platform SYLVIUS (Galgo Medical, SL and Hospital del Mar Medical Research Institute, Barcelona, Spain) [12], with support for both T1-Gd and DSA. This software allows the neurosurgeons to cooperatively visualize and manipulate neuroimaging data of the patient and the plan trajectories in a 2-dimensional and stereoscopic 3-dimensional virtual multimodal environment, allowing a better understanding of the anatomic relationships. Trajectories imported from the ROSA software were represented as 3-dimensional lines surrounded by tubular shapes indicating the diameter of the security zone (Figure 3.1). DSA and CTA, when available, were coregistered

to the T1-Gd volume using a mutual-information metric [88]. Coregistrations were visually verified. The neurosurgery team corrected the trajectories if needed, adjusting them with the mouse in the orthogonal cross-sections view, or with the stereoscopic stylus in the volumetric views.

3.2.3 Data gathering

The closest vessel to a trajectory was visually identified and labeled according to its distance to the trajectory axis in four categories (Figure 3.2 A-C). Vessels outside the security zone limit (>3mm from the axis) were labeled as belonging to "Zone A"; those at a distance between 2 and 3 mm belonged to "Zone B"; between 1 and 2 mm, "Zone C"; and closer than 1 mm, "Zone D." Modified trajectories with no visible offending vessel were collected inside "Zone A" as well. Vessels from "Zone D" posed the highest risk of vascular rupture during surgery since they might intersect the implantation trajectory. Vessels from "Zone C" are of high risk as well since they are within the reported median accuracy error for implantation [37, 89].

The magnitude of the modification was measured by the displacement distance in millimeter between "entry points" or "target points" before and after the revision.

The revision procedure as explained was performed by all the neurosurgeons (Ms. LS, IDM, and GC) to avoid interrater variability. The final consensual plan was transferred back to the ROSA[REG!!] software and verified once again by the chief neurosurgeon (GC) according to the manufacturer's guidelines to ensure the validity and safety of the surgery before implantation [90]. After that, the plan was transferred to the robot in the operating room for the implantation with no further modifications. No patient suffered complications derived from the surgery or the catheter angiography.

Descriptive statistics are shown as mean and standard error from the mean (mean $\pm$ sem) or median and first and third quartiles (median [Q1-Q3]). Statistical significance was calculated using the Wilcoxon signed-rank test, with P values <0.05 considered as significant. The analysis was carried out with the R statistics package (R Core Team).

A

Zone A (>3 mm): Outside the security zone — Low-risk
Zone B (2-3 mm): Boundary of the security zone — Low-risk
Zone C (1-2 mm): Accuracy error of implantation — High-risk
Zone D (<1 mm): Intersecting trajectory — High-risk

B

C
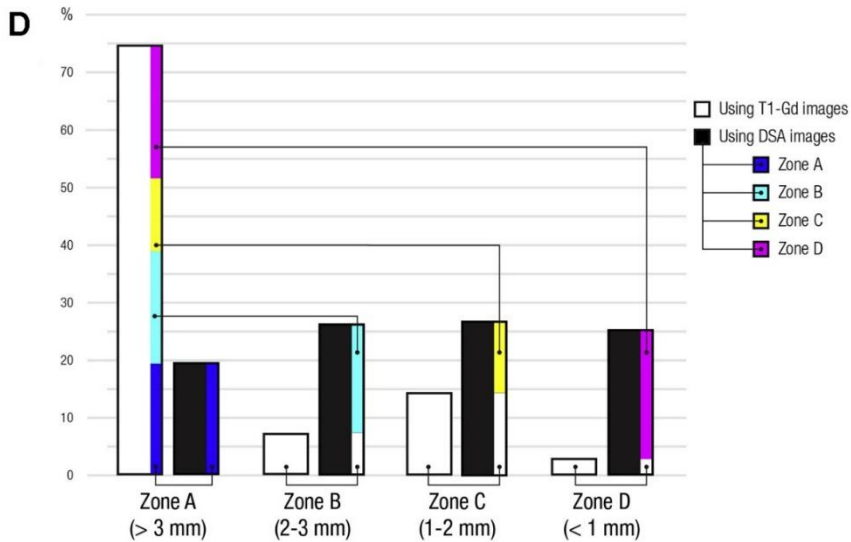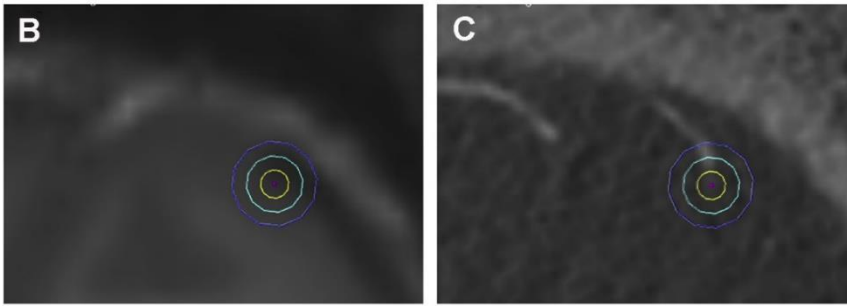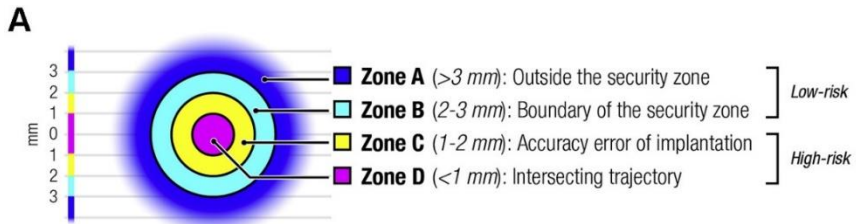
D Vessel discoveries in each proximity zone

Using T1-Gd images
Using DSA images
Zone A
Zone B
Zone C
Zone D

Figure 3.2 Security zone subdivisions (A) Scheme showing the different proximity zones and corresponding distances to the trajectory axis. (B and C) Example of a vessel discovered in Zone B of the digital subtraction angiography (DSA) imaging (B) but not seen in the T1-Gd sequence (C). (D) Percentage of vessels discovered in each proximity zones shown in the T1-Gd (white-filled bars) or DSA (black bars). Colors indicate the number of vessels labeled as Zone A in T1-Gd but found to be in the other proximity zones in the DSA.

3.3 Results

Twenty-two plans from subjects undergoing SEEG implantation surgeries were analyzed, comprising a total of 251 trajectories (11.4 trajectories per plan). Demographics of the patients (9 females and 13 males, median age 28.5) are described in Table 3.1.

Table 3.1 Demographics of Surgical Cohort

Case Num.	Age	Sex	Presumed EN	Laterality	Onset	Duration	AEDs	Past neurosurgical history	SEEG electrodes	Proposed Surgical treatment
01	28	M	Mesial temporal	Left	8	20	7		18	LITT
02	23	M	Posterior quadrant	Right	9	14	2	Subependymal Heterotopias	14	LITT
03	49	M	Insulo-opercular	Right	2	47	5		9	Resection
04	53	M	Posterior quadrant	Left	29	24	3		9	Re-examination
05	47	F	Mesial temporal	Left	22	25	4		10	Left AMTL
06	23	M	Cingulate	Left	15	8	5		14	RF-TC
07	30	M	Frontal	Left	14	16	6	Left frontal	11	Resection
08	42	M	Mesial temporal	Bilateral	14	28	5		15	RF-TC
09	30	M	Mesial temporal	Left	26	4	5		9	Left amygdalectomy
10	54	M	Frontal	Bilateral	9	45	2	VP-Shunt	8	Re-examination
11	23	M	Frontal	Left	14	9	4		13	RF-TC
12	32	F	Mesial temporal	Bilateral	13	19	3	Left AMTL	8	LITT
13	40	M	Posterior quadrant	Left	18	22	4		12	LITT
14	55	F	Mesial temporal	Bilateral	47	8	3		14	RF-TC
15	51	F	Mesial temporal	Right	47	4	3		8	Right AMTL
16	51	M	Frontal	Left	6	45	4		13	RF-TC
17*	48	F	Mesial temporal	Left	13	35	3		9	RF-TC
18*	47	F	Posterior quadrant	Left	26	21	4		10	Re-examination
19*	22	F	Mesial temporal	Right	9	13	4		12	RF-TC
20*	57	F	Mesial temporal	Left	28	29	3		8	Left AMTL
21*	27	M	Posterior quadrant	Bilateral	7	14	4		16	Resection
22*	38	F	Posterior quadrant	Left	6	32	5		11	Resection

EN: Epileptogenic network; AED: number of anti-epileptic drugs AMTL: Anteromesial temporal lobectomy; TBI: Traumatic brain injury; VP-shunt: ventriculoperitoneal shunt; LITT: Laser Interstitial Thermocoagulation; RF-TC: Electrical radiofrequency thermocoagulation.

Plans were initially built using exclusively the T1-Gd imaging since the robot's native planning software does not support DSA data. DSA was accessible only after transferring the plan to the SYLVIUS platform for the revision.

3.3.1 Revision with T1-Gd

During revision in the SYLVIUS platform using the T1-Gd sequence, the neurosurgical team identified gadolinium-enhanced vascular structures located on the boundary of the security zone or beyond in 81.6% of the trajectories (181 trajectories in Zone A and 19 trajectories in Zone B). In 14.3% of the trajectories they found vascular structures at <2 mm (36 trajectories, Zone C), which is the reported accuracy error of our system[89]. In the remaining 3.9% of the trajectories, a vessel was identified intersecting the trajectory (10 trajectories, Zone D). The reason why vessels were discovered during the revision with T1-Gd but not during planning, despite using the same image set, was attributed to display quality differences between the screens used for planning (the manufacturer planning laptop) and revision (a zSpace system running SYLVIUS). However, we did not consider it necessary to backtrack those vessels in the planning laptop to verify this assumption.

3.3.2 Revision with Digital Subtraction Angiography

Reexamination of those same plans using DSA in the SYLVIUS platform showed that only 19.5% of all trajectories (49 trajectories) were avascular, namely the closest vessel was found beyond the security zone (i.e., in Zone A (Figure 3.2D). That is to say, DSA revision revealed vessels in 132 out of the 181 trajectories labeled as Zone A using T1-Gd (72.9%). A vessel within the accuracy error distance (Zone C) was identified using DSA in 27.8% of all trajectories (70 trajectories). Vessel-intersecting trajectories (i.e., those trajectories with vessels in Zone D) were detected in 25.9% (65 trajectories) of the cases. A 73.1% of the vessels found in Zones C or D were located intraparenchymally, at an average depth of 10.8 mm ± 1.7 mm.

As consequence of the new information provided by the DSA, an average of 81.4 ± 4.6 % trajectories from each plan were corrected.

More than half (67%) of those corrections consisted of combined modifications of both the entry and the target points. In the remaining corrections, a shift of either the entry point (26.4 % of the corrections) or the target point (6.6 % of the corrections) was sufficient for finding an avascular path. Overall, the neurosurgeon could find a suitable path close to the original one, therefore preserving the diagnostic aims of the original plan. The magnitude of the modification was similar in either point (median value of 5.43 [3.10-12.12] mm for modifications in the entry point and of 6.86 [4.83-11.99] mm in the target point, paired Wilcoxon test P = 0.94).

3.3.3   Revision with CTA

Six of the plans (66 trajectories) were additionally revised with CTA since they were the only ones with all T1-Gd, DSA, and CTA available (Table 3.1).

CTA examinations resulted in a mean dose-length product (DLP) of 1.9 ± 0.2 Gy $\cdot$ cm, corresponding to an effective dose of 3.61 ± 0.46 mSv. The mean fluoroscopy time for those same patients during the DSA examination was 248.9 ± 23.9 seconds. The total dose-area product was 48.1 ± 5.5 Gy $\cdot$ cm^2, corresponding to an effective dose of 4.19 ± 0.48 mSv. The effective dose of DSA was not found to be greater than the one of CTA (paired Wilcoxon's test p=0.24).

During the revision of these 6 plans, 50 trajectories were assigned to the Zone A group using T1-Gd imaging. Most (84%) of those trajectories (41 out of 50) were confirmed to be vessel free as well in the CTA. However, revision with DSA found vessels in 70.3% of the trajectories labeled as Zone A in the CTA (i.e., 29 trajectories contained vessels inside the security zone that were identified in the DSA data but not in the T1-Gd or in the CTA data). The rest of the findings indicated that the discrimination of vessel structures near planned trajectories by the neurosurgeon was similar when using either CTA or T1-Gd.

3.4   Discussion

Vessel rupture during electrode implantation is one of the most severe complications of SEEG surgery[68]. After the initial 547

electrode implants (51 cases) in our center, we had to regret 2 acute bleeding episodes, the last one causing irreparable damage to the patient with a permanent moderate hemiparesis in spite of immediate craniotomy and acute subdural hematoma evacuation. In both cases a pial artery was the cause of bleeding in our series. We identified the cause in both cases as a failure to identify a dural vessel in the double-gadolinium contrast enhancement T1 preoperative implantation plan since the vessel did not show up in the images. This fact led us to consider the use of DSA in every planning and motivated the realization of this study.

3.4.1 Digital Subtraction Angiography provides certainty about vessels with higher rupture risk

To prevent vessel rupture during implantation, we try noticing the presence of intraparenchymal vessels through palpation during the advancement of the electrode into the parenchyma. Vessels are on occasions revealed during the insertion of the probe and the electrode by a slight opposition to the smooth inward movement. Arterial vessels may be felt in this manner as structures of more rigid and rubbery consistence than the parenchyma. On the few occasions that we were able to experience this by palpation, we aborted the implantation of the electrode. Later, the various neuroimaging post implantation coregistration examinations seemed to indicate that there were vessels at those locations.

Vessels with the highest risk of being punctured during implantation are in our opinion not those large intraparenchymal vessels, which may be identified by palpation, but the superficial ones since they are susceptible to be damaged, in our opinion, during the skull perforation and dura mater manipulation (Figure 3.3B). Despite the placement of stops on the drill bit to prevent it from going beyond the thickness of the skull, we think that rotational violence of the drilling while traversing the bone may occasionally injure the underlying parenchyma, rupturing underneath surface vessels. Consequently, we are extremely careful during planning and revision to the detail of the meningeal vasculature underneath the entry point. In our experience, double-gadolinium contrast enhancement T1 seems to show better veins than arteries [91]. Moreover, it is often unable to show vessels

close to the cranial vault, either because of resolution or contrast limitations, unspecific and confounding contrast enhancement of the dura mater, and magnetic gradient distortions near the bone.

Figure 3.3 SYLVIUS use in clinical practice   (A) Neurosurgeon using the stereoscopic display and 3-dimensional interaction tool during the revision of an implantation plan in the SYLVIUS platform. (B) Bone drilling during the electrode implantation. The neurosurgeon keeps an eye on the overhead monitoring displaying the implantation plan with the digital subtraction angiography and T1-Gd.

3.4.2 Complications of Digital Subtraction Angiography and SEEG interventions must be balanced

Several studies have shown a global incidence of DSA related complications as high as 2.6% and a risk of permanent damage of up to 0.5% [80]. The complication rate is considerably reduced in young healthy subjects with no history of cerebrovascular disease [92, 93], which also applies to subjects undergoing SEEG procedures [25]. Several reference centers in both the United States and Europe have already incorporated DSA imaging in their SEEG operative workflow and encourage its use [94, 95]. But nevertheless, the necessity of bringing a new risk to the patient needs to be carefully balanced. Our reported findings suggest that a certain number of complications related to SEEG vascular rupture could be a consequence of unobservable vessels in the T1-Gd, and therefore

they may be avoided by identifying vascular additional trajectories using DSA.

3.4.3 Use of alternatives to Digital Subtraction Angiography

Unfortunately, DSA is an invasive test that is not exempt from complications. Various other magnetic resonance sequences (e.g., time-of-flight imaging, CTA) have been proposed as safer alternatives for imaging of brain vessel structures[77]. In our study, CTA was available to the neurosurgeons for reviewing the plans only in the last 6 patients.

DSA interventions are reported to produce 5 times higher radiation exposure when compared with CTA [96]. For that, diverse techniques have been proposed to reduce the radiation exposure during the examination [97]. Our calculated total effective dose for the complete DSA intervention (4.19 ± 0.48 mSv) was higher but not far from the one calculated for the CTA examination (3.61 ± 0.46 mSv). Both DSA and CTA doses were slightly lower that the ones communicated in similar studies [98]. From here we can conclude that the risk of radiation exposure of performing a diagnostic DSA for SEEG planning is only slightly higher that using CTA instead.

Compared with CTA or T1-Gd, DSA offers a decisive advantage for vascular identification. Most of the alternative examinations result in a poorly contrasted vasculature at the meningeal layers (Figure 3.4 and Figure 3.5). In contrast, DSA allows us to identify unequivocally both meningeal and intraparenchymal vessels, even those of submillimeter caliber. Our findings corroborate the usefulness of DSA for SEEG planning. In at least 2 out of 3 trajectories, DSA imaging evidenced vessels inside their security zone that lacked contrast enhancement in either the T1-Gd or CTA.
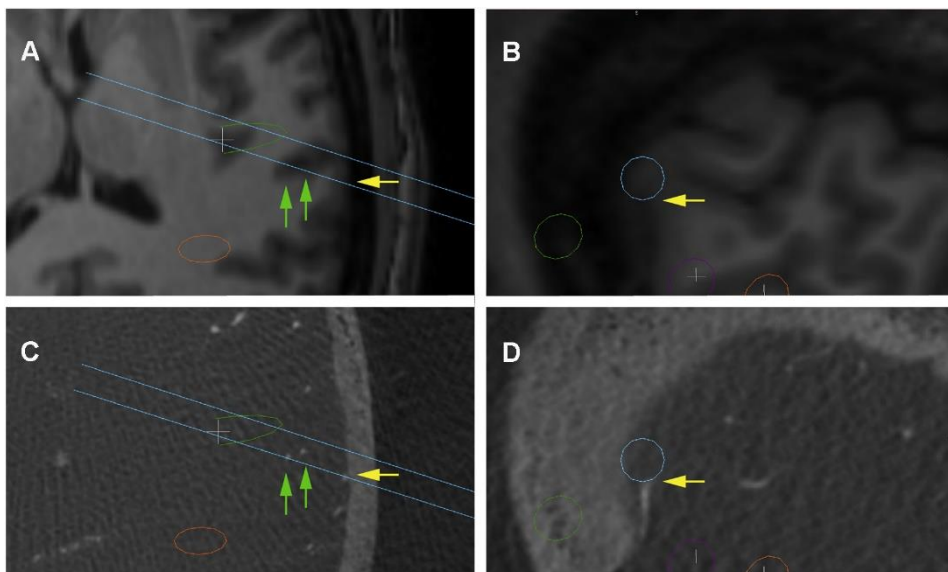
Figure 3.4 Example trajectories containing vessels. A meningeal vessel (yellow arrow) and intraparenchymal vessels (green arrows) in a T1-Gd sequence (A and B) and digital subtraction angiography (C and D). The proximity of the vessel to the bone may add rupture risk during drilling.

3.4.4 Strategies to use Digital Subtraction Angiography information for planning

Another much debated question is whether the vascular network displayed with DSA may be too overwhelming, causing the neurosurgeon to choose less diagnostically relevant trajectories out of excessive cautiousness [81]. Our measurements show that the neurosurgeon had to reposition both the entry point and target point, which indicates an elaborate 3-dimensional manipulation. Vascular models generated from DSA data are highly detailed and therefore extraordinarily complex. The search for avascular trajectories is certainly a quest. The neurosurgeon cannot rely solely on 2-dimensional shifts using the orthogonal views of the planning software; he or she must think tridimensionally, moving the path as a whole, checking different orientations until finding the proper way. Here we used the SYLVIUS platform, a new planning software being validated in our institution, to provide the neurosurgeon with a natural interface with which to manipulate such complex data: a stereoscopic display and 3D interaction tools during the revision (Figure 3.3A). The advantage of this approach is that it allows the

neurosurgeon to visualize and manipulate the neuroimaging data and plan trajectories in a virtual multimodal environment, allowing a better understanding of their anatomic relationship. The neurosurgeon seemed to react only to the presence of vascular structures within the security zone, regardless of the source of the data being visualized. Thanks to this, neurosurgeons were able to find alternative safe paths within the vicinity of the originally planned ones. For this study we did not use computer-assisted planning algorithms [28, 42, 60, 99, 100], letting the neurosurgeon the decision and responsibility for correcting the plan. Those algorithms search for avascular paths automatically based on a certain number of constraints. The combination of computer-assisted methods and hand manipulation of surgical plans with stereoscopic displays will certainly simplify the creation of implantation plans and increase its safeness.

3.4.5 Limitations in the Use of Digital Subtraction Angiography for SEEG Planning

Despite the fact that our neurosurgical team benefits from the use of DSA during the revision pipeline to identify vessels under risk of being pierced by an electrode implanted through a certain trajectory, we cannot assess with certainty when a trajectory may cause vessel rupture. Recent studies have retrospectively shown that a significant number of electrodes are implanted through vessel-intersecting trajectories without any consequence [74]. It is not clear what morphologic characteristics pose the highest rupture risk for a vessel when hit by an electrode. In earlier surgeries we have occasionally ignored vessels that were deeply buried in the parenchyma or too small in diameter and/or running parallel to the trajectory without intersecting it, or even if they were inside the security zone, without detecting any bleeding problem. Knowing with precision the rupture chance of a vessel found during revision with DSA would be extremely useful to assess the real risk.
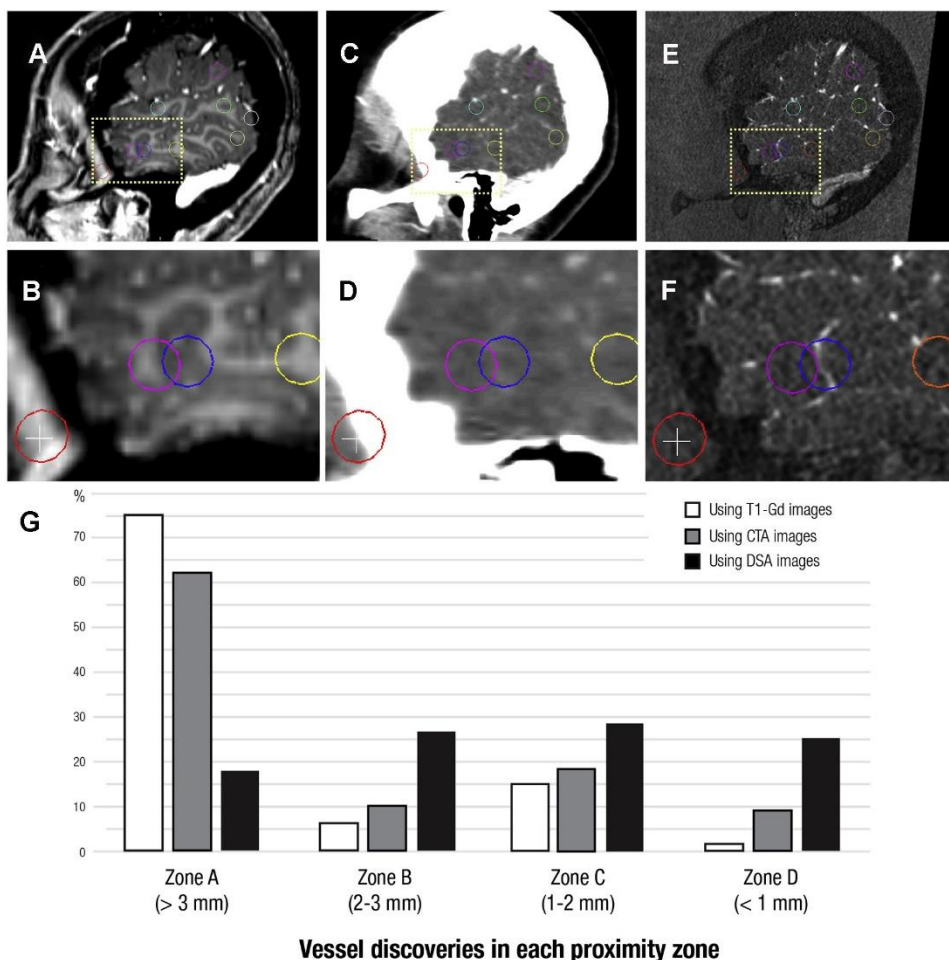
Figure 3.5 Different modalities comparison. Vessel intersecting the blue trajectory as visualized in 3 different imaging modalities: T1-Gd (A and B), computed tomography angiography (CTA) (C and D), and digital subtraction angiography (DSA) (E and F). Panels on the right correspond to the yellow inset box from the panels in the left column. Colored circles show the security area of the different trajectories. (G) Percentage of vessels discovered in each proximity zones shown in the T1-Gd (white bars), CTA (gray bars), or DSA (black bars) for the 6 patients for which all 3 modalities were available.

Our study cannot exclude that noninvasive neuroimaging modalities may serve the neurosurgeon similarly to DSA. Our findings support that a detailed vascular visualization such as that given by DSA should be used when possible to provide the neurosurgeon the best information possible to safely plan the implantation.

3.5   Conclusions

Use of DSA in addition to T1-Gd during the revision of SEEG procedures allowed our neurosurgery team to identify a higher number of vessel-intersecting trajectories that were otherwise not seen. The highly dense vascular tree shown by DSA requires complex strategies to circumvent the vessels, but such corrections do not modify the plan's original diagnostic aim. This study provides support for routine use of DSA for planning SEEG procedures, the potential of which to prevent vessel collisions during electrode implantations might outweigh the risks of catheter angiography.

4 COMPUTER ASSISTED PLANNING

4.1 Introduction

Around one-third of epileptic patients do not respond to antiepileptic drugs [19] and could be treated with epilepsy surgery [101]. Stereo-electroencephalography (SEEG) is a stereotactic technique used in complex drug-resistant epilepsy cases to evaluate a possible surgical intervention [26, 27, 37, 68]. This is an invasive technique that consists of the placement of several rectilinear depth electrodes. It is used to measure electric fields inside the brain with the multiple contacts in a row placed in each trajectory [102].

SEEG is an invasive technique that is performed on selected patients to answer clinical questions when a clear chance for a surgical solution is feasible, and previous noninvasive information is not enough to elucidate proposed options for depicting the epileptogenic zone (EZ) and epileptic network. This noninvasive patient information includes seizure semiology, especially the initial symptoms that appear at seizure start, neuropsychology testing, MRI, video EEG recordings, and frequently PET scanning and ictal and interictal (and SISCOM) information. It may be difficult to understand the onset area from video-EEG surface electrodes recordings (mostly when it is deep as for instance if it originates from the insula, the orbital frontal, the mesial structures as the cingulum), or to elucidate the side of seizure onset in a rapidly generalizing seizure.

The implantation of SEEG requires careful planning of the trajectories. The SEEG trajectory plans evolve from an initial draft which evolves in successive degrees of refinement until a final

surgical plan is obtained. SEEG has a strong multidisciplinary component [103, 104], with epileptology and neurosurgery being the most involved clinical specialties. In this document, we use the term *initial plan* to denote a concept similar to the 'epileptologist plan' [12, 105] or 'the strategy of the implantation' [46, 106] mentioned in related literature.

The initial steps of the SEEG workflow that is carried out at Hospital del Mar, Barcelona requires the epileptologists to suggest an initial trajectory plan based on an EZ localization hypothesis based on non-invasive clinical information. Following that initial plan from the epileptologist, neurosurgeons modify the initial plan looking for safe trajectories, taking into account the new information incorporated about cerebral vascularization (e.g., DSA or CT scans) and adapt that plan for surgical safety [12]. The work presented here starts right after the epileptologist has provided its initial trajectories, and it is aimed at aiding neurosurgeons with tools to early detect and discard high-risk trajectories and find alternative ones when required.

There is consensus that the most important risk to avoid is intracranial bleeding [26, 68, 107] which can cause significant damage or death. Special attention is taken to avoiding vessels at the beginning of the trajectory in the cortex, as they are associated with greater bleeding risk [105]. Surgical planning is patient-dependent and has been described as a time-consuming and inefficient process [108]. It may involve the visual inspection of multiple 2D slices from 3D imaging datasets so that a cylinder shape that surrounds the electrode, commonly referred to as the security zone (SZ) is free of vascular structures to be avoided. During the rest of the manuscript, the SZ is defined by the diameter of the cylinder that has the trajectory as its main axis. The SZ used depends on the precision of the implantation device (e.g., surgical robot) and institution/clinician criteria.

Previous work in stereotactic automatic planning has been presented for Deep Brain Stimulation (DBS) [109], needle biopsy [110, 111], SEEG [40, 47] and other straight-access neurosurgical interventions [112, 113]. For procedures where only the tip is active (e.g., DBS, needle biopsy, or laser ablation) a common approach is to compute the optimal entry point given the desired target defined by the user.

However, this strategy is not entirely sufficient for SEEG electrodes, which measure electrical data along its entire length.

Specifically for SEEG planning, the Milan group presented a method that takes into account the distance from vessels, sulci avoidance, and penetration angle based on the user selection of one target point and an entry region [40]. The method was later modified [100] so that the user selects a rough entry and a rough target. This work was further developed to optimize trajectories [105] computing for each trajectory all possible entry-target combinations from within a user-defined entry and target permitted areas, where the exact number of candidate entry and target points was defined by image resolution. In its evaluation study clinicians were asked to rank qualitatively (either 'good', 'acceptable' or 'discarded') the *adherence* of the alternative trajectory to the initial one, both at the entry and the target regions. In a later work from the same group, a new method was presented with an increased computational speed of 160±102 s/trajectory [108]. To increase safety, a Maximum Intensity Projection (MIP) method was presented which takes into consideration the first centimeter of the trajectory [42].

Epinav™ is another software platform for automated SEEG planning, reaching interactive rates for finding alternative entry points for a given target point. Then a method is presented which is dependent on the skull mesh segmentation results to initialize the search [47]. More importantly, the method searches for the best entry point for a given target but cannot be used to search for the best target point for a desired entry. It makes fast computations using the GPU (5000 candidate entry points in ~250ms). Epinav™ also has a visualization tool that provides a graph for each trajectory in which the horizontal axis represents the length of the electrode, and the vertical one represents the distance to the nearest critical structure in any direction. Later in [114], a multiple trajectory planning algorithm was presented which, takes into consideration the amount of gray matter traversed to increase electrode efficacy, apart from considering electrode collisions. The reported time was below a minute for 7-12 electrode plans. Regarding alternative path computations, results are displayed with a color-coding directly on the skull surface, similarly

to other tools published for DBS [115], needle biopsy [110, 111], and general keyhole neurological interventions [5, 56, 112, 116].

Zelmann et al. [117] presented another method that also considers the location of individual contacts to maximize recording volume while constraining the trajectories to safe paths, considering a wide variety of constraints. Only 3 target structures per hemisphere were considered (1 in the amygdala and 2 in the hippocampus) and a distance map is computed from the surface inwards to represent the greater importance of measuring from the center of the structure. Gaussian sampling was used to sample possible target points from segmented deep target structures and possible entry points from the entry regions to favor the evaluation of trajectories traversing central areas. On average, 7 minutes per optimized trajectory was reported.

Most of the described approaches focus on adhering to the distal target (e.g., hippocampus). However, the proximal entry point of the brain is sometimes critical in SEEG. This entry point may be crucial to measure from an identified structural lesion (e.g., abnormal brain tissue) or a superficial functional cortical region such as Broca's or Wernicke's [104, 118]. Although adherence to the entry or the target has been used for qualitative alternative evaluation, but to the best of our knowledge it has not been used as an input to the optimization. Furthermore, adherence to the *insertion angle* is yet another form of adherence that might be useful for SEEG approaches (such as [119]) in which all trajectories are as parallel as possible to each other. Thus, there is a need for an automated trajectory planning tool that takes as input different approaches to maintain adherence to the initial plan, and which performs at interactive rates.

4.2 Method

In this section, the two tools used by our method, the Depth Map and the Alternative Finder, will be described, as well as their integration with a GUI and its experimental evaluation. A combination of projective geometry and distance map computation is used to transform the 3D problem into the 2D domain to simplify the problem and speed up computation.

The tools will be presented to avoid volumetric no-go zones (i.e., vessels) which we will refer to as the *mask volume*. This mask volume is obtained by registering and merging all DSA datasets into one and then performing a threshold segmentation. Those DSA datasets contain venous and arterial information of each patient (two for each implanted brain hemisphere). Nevertheless, the described functionality can be used with other datasets and can be adapted to consider go zones and/or mesh inputs. The description also assumes that the datasets are contained in a scene graph data structure and are registered via relative transformations [48, 120].

4.2.1 Depth Map tool

The Depth Map tool accepts two inputs: a mask volume containing no-go zones and a trajectory. The tool is designed to early detect and visualize critical structures within the SZ of the trajectory. It works by projecting the portion of the mask volume contained inside the trajectory SZ into 2D space to create a *depth image,* which contains depth information for each rendered pixel. Later, that depth image is evaluated to find 'cylindrical SZ vs. no-go zone' collisions. This procedure shares similarities with the MIP implementation presented in [42]. A preliminary version of this tool was presented in [60] and mentioned in [120].

To obtain the depth image, a rendering pipeline needs to be configured. First, a mask volume is positioned in object space with a transformation parametrized by several DICOM tags (e.g., pixel spacing, image orientation). Then, it is multiplied by its model transform T_{model}, obtained by concatenating all its ancestor relative transformations contained in the scene-graph, which again modifies its pose (i.e., translation and orientation) placing it in *world space* (i.e., registered). The view transform T_{view} is then applied, leaving data in *camera space,* which is centered at the entry point facing the target point. The next step is to apply an orthographic projection T_{proj} defined by the smallest square prism which fits the cylindrical security zone of the trajectory (). After that perspective division takes place, and finally, the viewport transform $T_{viewport}$ maps the result to the final 2D image (resolution of 128×128 pixels).

After the rendering, the depth image (i.e., z-buffer) is retrieved. A non-linear look-up-table (LUT) is used to map each value of the depth image from black (far clipping plane) to a solid color (near clipping plane). The pixels inside the circumference that are not black (i.e., depth different than the far clipping plane) represent vessels inside the SZ. The algorithm takes advantage of the volume rendering capabilities provided by VTK [121].

An approximate formulation of the order in which each step is applied can be represented by the following equation:

$$2D\ Depth\ map_{image\ space}$$
$$= T_{viewport} * Perspective\_divide(T_{proj} * T_{view}$$
$$* T_{model} * 3D\ Volume_{object\ space})$$

Radial distance to critical structures is preserved under the orthographic projection, allowing for the computation of the distance from closest vessel to electrode axis by measuring the closest non-null pixel to the 2D depth image center. The span of the trajectory can be subdivided (e.g., entry region and rest), allowing for the computation of vascular distances on each subpart of the trajectory. Please note that in this tool and the rest of the manuscript, distance to vessels is expressed in diameter, instead of radius, to comply with the SZ definition used in some robotic implantation systems.

4.2.2 Alternative Finder tool

This tool also takes as input a mask volume containing no-go zones and a trajectory. Its purpose is to find alternative trajectories (i.e., trajectories without vessels inside the SZ) that adhere to a given initial trajectory. The metric to decide what is closer (or more adherent) is selected by the user from among three available options: trajectories with *similar entry*, *similar target*, or *parallel* (with the same angle relative to world coordinates).
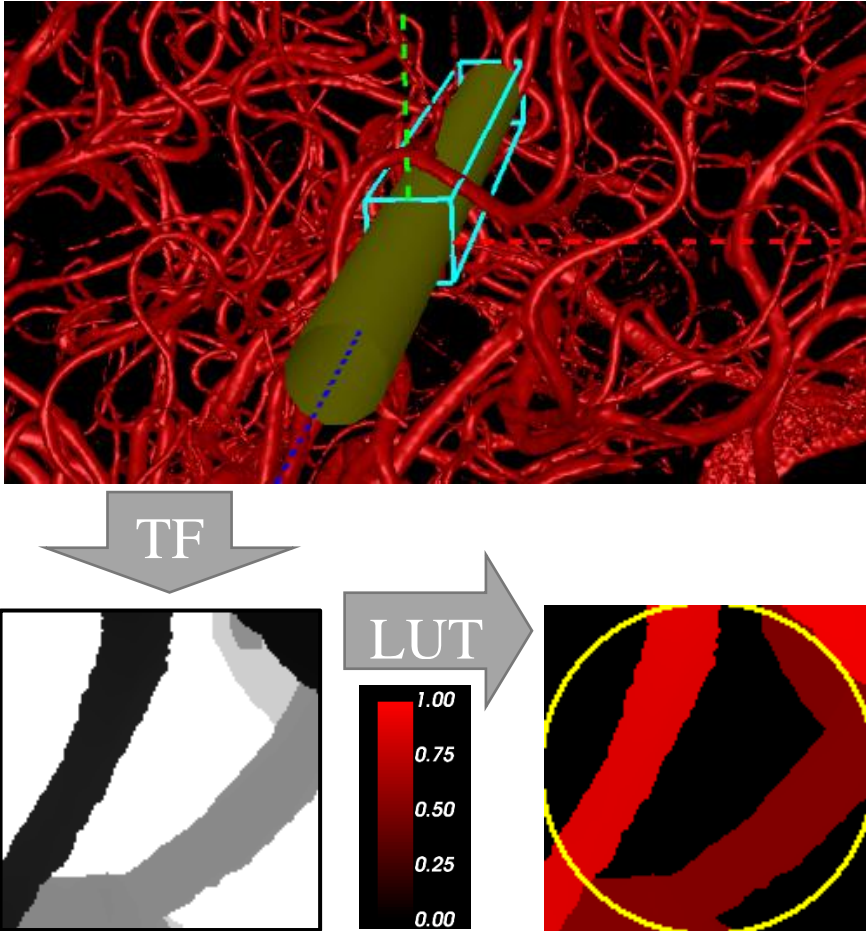
Figure 4.1 Volume rendering of one of the angiographies (i.e., vessel mask volume) depicting a cylindrical security zone in yellow and an orthographic frustum in cyan (top). Depth image in black and white (bottom left) and final image used in GUI (bottom right), both with a non-linear color mapping to enhance visualization. The 3D cylindrical security zone is prolonged towards the outside of the head for clinical visualization purposes.

In contrast with the Depth Map tool, where each depth image computation allowed for the computation of one trajectory, the Trajectory Finder computes for each render as many trajectories as pixels contained in the 2D depth image (currently 128×128 pixels, resulting in over 16K alternatives/depth image).

First, the Signed Mauer distance map algorithm [122] is used to create a distance map from the binary image. A transfer function is created and configured with a Boolean predicate function, mapping

1 (fully opaque) to values smaller than the SZ radius of the trajectory, and 0 (transparent) to those above it. When visualizing the distance map with that transfer function, a fattened version of the vessel tree appears. The reason to perform this operation is that finding vessels inside the security zone (this time defined by a capsule instead of a cylinder) is equivalent to finding the intersection between line segments and the threshold distance map described (Figure 4.2).
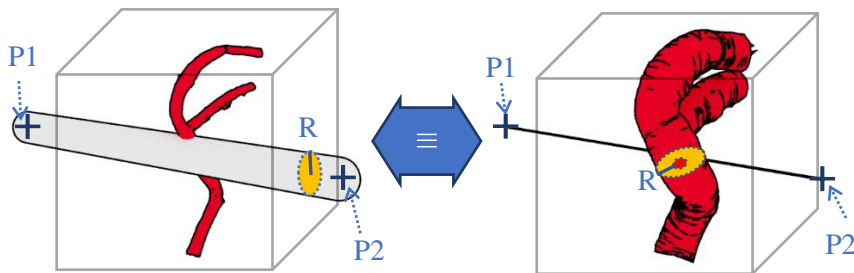
Figure 4.2. Transfering the SZ to vessels. Computing if a path's security zone (defined by a capsule) hits the vessel (left) is equivalent to computing if the line segment P1P2 hits the enlarged vessels (right).

The parametrization of the rendering is the same as in the Depth Map tool, apart from the location of the camera, and the use of orthographic (parallel) or perspective (similar entry/target) projection (Figure 4.3), which depends on the adherence strategy selected:

- *Similar entry*: a perspective camera located at the entry point facing towards the target point. Field-of-view is set to 15°.

- *Similar target*: same as the previous one but located at the target point facing the entry point.

- *Parallel*: same parameters as in the previously described step. Resolution and lateral frustum bounds could be modified to affect trajectory density and search space.
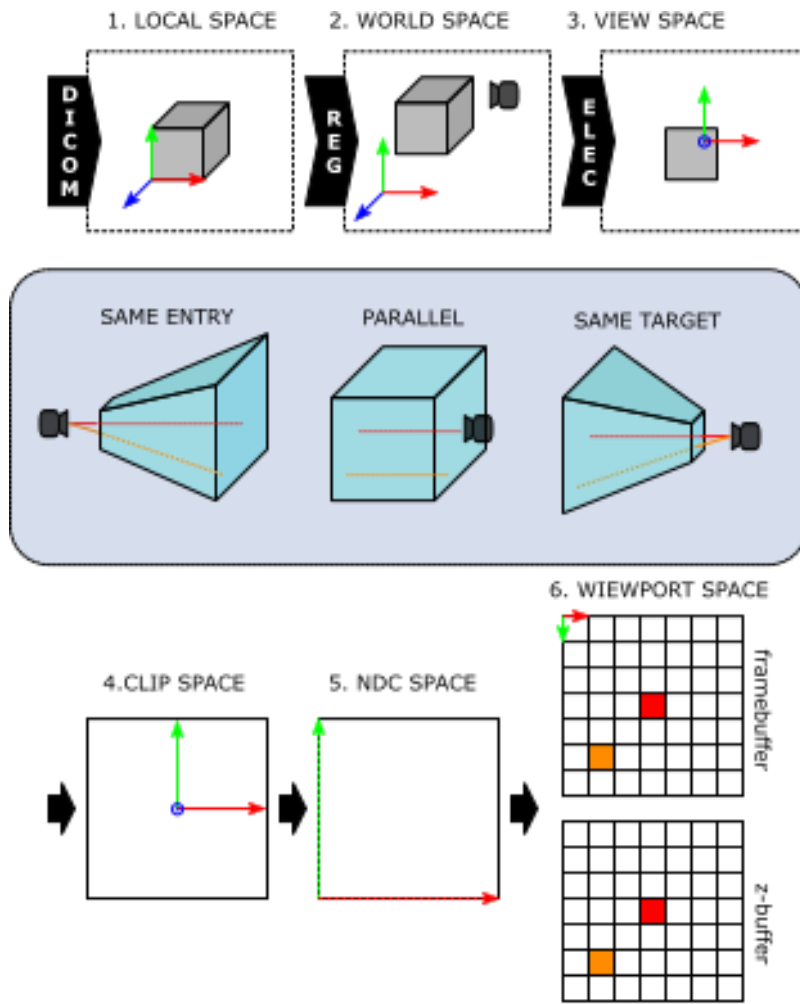
Figure 4.3. Graphical pipeline parametrized to compute electrode trajectories.. In 3 different setups, 2 line segments (red and orange) are projected by different frustums, yielding the same final 2D image in viewport space. In all three cases, each trajectory gets collapsed into points/pixels.

After the rendering, depth is recovered, where each pixel with a value of 0 represents an avascular trajectory with no vessels inside its SZ, (P2 in Figure 4.4). Then, the closest 0-value-pixel from the image center (P1 in Figure 4.4), if found, is used to compute its associated trajectory. For that, all pose transformations described for the Depth Map tool must be applied to P2 in reverse order.
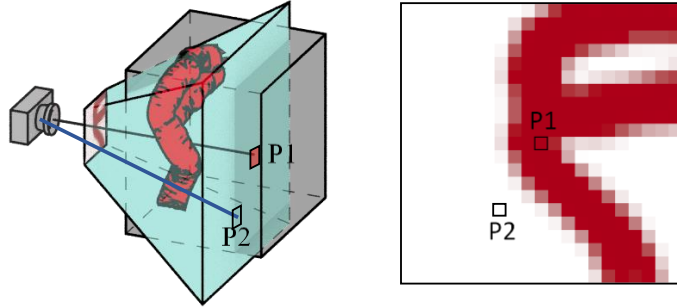
Figure 4.4 On the left, a 3D distance map is rendered with a perspective frustum. On the right, the final rendered image. P1 depicts the central pixel (which signals vessels inside the initial security zone) and P2 one possible avascular path.

In the *similar entry* strategy, when an alternative is not found in the first render, the search continues moving the entry (P$_0$), spiraling away on each iteration (n) in a plane perpendicular to the trajectory, following a pattern (Figure 4.5) described by the following formula (were radial distance (RD) is 0.1 mm and ω is ~135.5º, an approximation of the golden ratio in the angular form):

$$P_n = P_0 + RD * n * e^{i\omega n}$$

With:

$$n \in [0, n_{max}]$$

Where:

$$\max(\Delta P) = |P_n - P_0| = |RD * n_{max} * e^{i\omega n_{max}}| = RD * n_{max}$$

A new set of trajectories are evaluated for each iteration, and the search stops as soon as one avascular trajectory is found, or a maximum number of iterations (n$_{max}$ =32) is reached. The similar entry points lie on an Archimedean spiral and are visited in order (from the inside to the outside), with higher density near the initially selected entry (Figure 4.6). The *similar target* strategy provides equal functionality but moving the target instead.
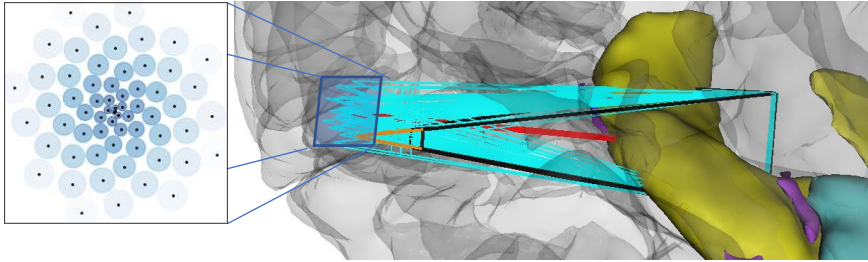
Figure 4.5 Spiral pattern for modifying the entry or target point (black dots) in the similar entry/target strategies. Each new point is 1 RD further away from P0 than the previous one, rotated another ~135.5º, resulting in a bigger density towards the center. Two frustums (orange and black) are used to examine each subset of trajectories. The smaller orange frustum shows the one used for the computation of the entry-SZ constraint (7 mm), while the black one is the one used for the general SZ (5 mm) requirement. The preliminary trajectory is depicted in red.

When more than one mask volume or mesh is available (e.g., DSA volumes for arteries or veins considered separately), each dataset is projected individually, and the resulting depth images are aggregated before the closest risk-free trajectory selection. The same approach is used when considering different SZ requirements along the length of the trajectory. This situation is depicted in Figure 4.5, where two frustums (an orange frustum for the entry region and a black frustum for the rest of the electrode) are used to search for vessels at different subsections of the trajectory.
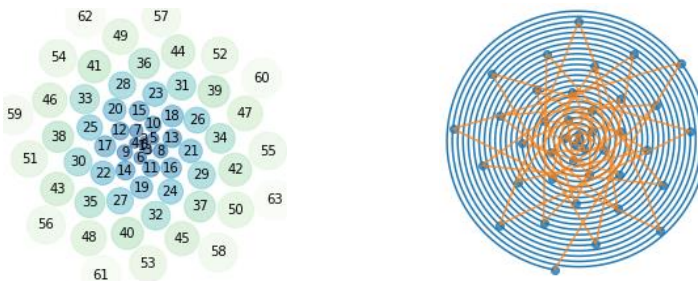
Figure 4.6 Spiralling pattern. Left: order of the points visited, with bigger density near the centre. Right: same points lying on the Archimedean spiral.

4.2.3 GUI – Integration with a surgical planner

The method has been integrated into SYLVIUS [120], a SEEG surgical planning system designed specifically for epilepsy surgery. The Depth Map tool is controlled by the user with the interface

depicted in Figure 4.7. Here, information obtained from a DSA acquisition is used to provide the vascular structures. For each trajectory, the interface lists the avascular SZ diameter (i.e., twice the radial distance to the axis). The interface also signals collision with other SZ, which is computed by projecting the meshes of every other trajectory (green screen when no collisions, greyscale otherwise).

When the user clicks on any vessel on the DSA image seen along the trajectory of the electrode, the 3D and tri-planar views get centered at that point for user inspection. For that, the transformations described in the previous section must be computed in reverse order, starting from the 2D image coordinates and its corresponding z-value, all the way back to world space. Please note that this requires the depth value, which is normally lost in normal rendering and MIP.

If a trajectory is found to be unsafe with the Depth Map tool, the Alternative Finder tool can be configured with different avascularity requirements for the entry region (first 6 millimeters) and the rest of the trajectory. It can also be instructed to search for alternatives with a specific adherence strategy. When a trajectory is selected, only close by vessels are depicted in the 3D view to facilitate visual inspection.
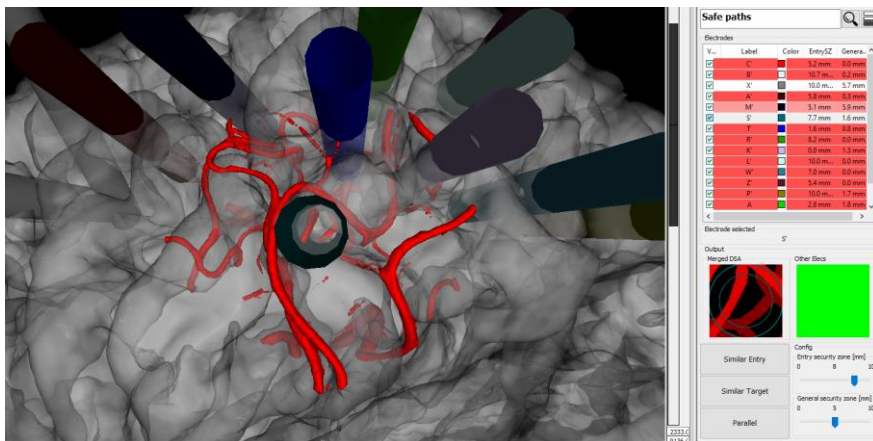
Figure 4.7. GUI integration. Left: 3D view with mask volume (i.e., DSA) only displayed around the selected electrode. Right top: entry and general SZ computed for each electrode. Right bottom: Selected electrode S' projected with a security zone of 8 mm in the entry and 5 in the rest. No other electrode in the trajectory is denoted by the green screen.

4.2.4 Experimental Design

To retrospectively evaluate both tools, a set of 12 patient cases requiring SEEG implantation was used. The cases were from Hospital del Mar, Barcelona (part of EpiCARE, the European Reference Network for epilepsy treatment) and contained preliminary and unrevised plans imported from two robotic platforms: the ROSA® (Zimmer Biomed Inc.) and neuromate® (Renishaw plc.). Electrode coordinates were imported referred to T1-weighted double-contrast Gadolinium T12c images (Philips Medical Systems, 256×256×100 image resolution). The cases were then co-registered within SYLVIUS with their DSA datasets (Philips Medical Systems, 256×256×256 resolution) and stored in a scene-graph data structure [120]. The registered DSA datasets (up to 4 for each case) were fused to produce a single 3D volumetric image. A threshold to segment vessels was then manually selected by a trained neurosurgeon, obtaining the vessel mask volume.

For each initial trajectory, the Depth Map tool was used to locate vessels inside the SZ. When vessels were found, Trajectory Finder was used to find alternatives. Depth Map was used once again to measure the alternative avascular diameter for comparison. The experiment was conducted on a laptop equipped with an Intel® Core™ i7-4810MQ CPU at 2.80GHz, and an NVIDIA Quadro K3100M GPU. Collision with other electrodes was not considered in the experiment.

The avascularity constraint was set to 7 mm in diameter for the first 6 mm of the trajectory (entry-SZ), and 5 mm diameter along the rest of the electrode. The number of electrodes that were already safe under that criteria, the ones with no alternative found, and the ones with alternative paths along with its type were recorded. To measure the adherence to the initial plan for each re-planning strategy, the Euclidean distance from the original and alternative entry and target points was computed. The re-planning computation time was also recorded for each trajectory and adherence strategy.

4.3 Results

The alternative trajectories obtained following the described experimental design are shown in Figure 4.8 arranged by the re-planning strategy used. For each alternative found, the avascular diameter measured for the initial (black) and the alternative (red, green, and blue) is shown, with an arrow connecting them. Distance to vessels is expressed as an equivalent avascular SZ diameter (twice the radial distance) for compatibility with the SZ convention used in the ROSA® and neuromate® robotic planning software.

A histogram with the Euclidean distance between original and alternative entry and target points is displayed for each re-planning strategy.
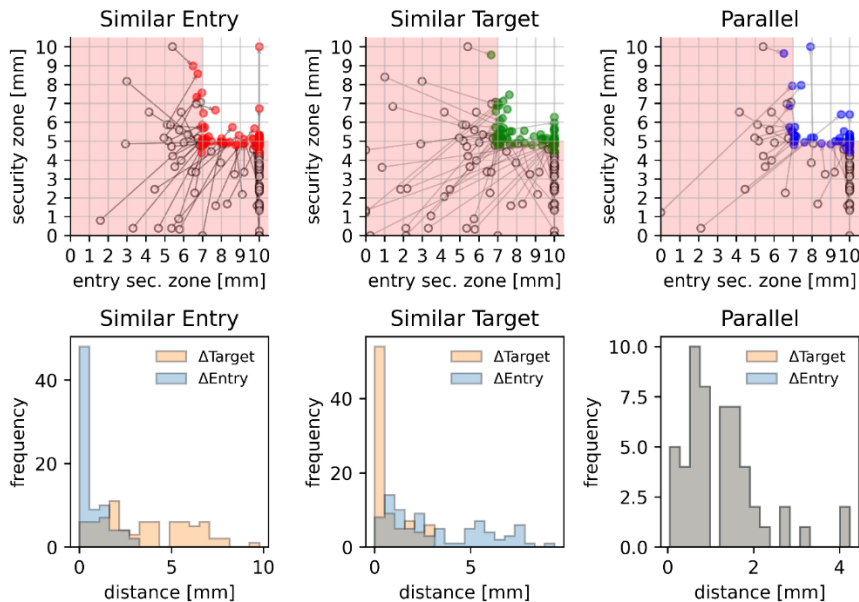
Figure 4.8 Alternative Finder results. Above: Diameter of the trajectory security zones for original trajectory (empty white circle), and after the computation (red, green, and blue circles). A white square on the upper right corner depicts the area with acceptable SZ values. Below: histogram of the Euclidean distance between the original and safe path, for the target (red) and entry (blue) points.

When an alternative was found, the average computation time was 77 ms per trajectory, with 75% of cases under 85 ms, and a maximum computation time of 765 ms. When no alternative was found, the time ranged between 8 and 889 ms. The average number of trajectories

computed per millisecond was 1781 (with a central 50% of 1638-2028). Information regarding the total number of electrodes found in each case, its type, and computation times can be found in Table 4.1

Table 4.1 Trajectories studied with preliminary plans, detailing the type of alternative found, computation time, and the total number of alternatives computed (7mm entry sec. zone, 5mm sec. zone).

Case	Elecs.	Already safe	With alternatives	Alternative strategy			Computation	
				Similar entry	Similar target	Parallel	Paths evaluated	Time [ms]
#1	10	1	8	7	7	5	8290304	4240
#2	14	7	7	7	7	7	2555904	1483
#3	8	4	4	4	4	4	1064960	750
#4	9	1	7	5	7	5	5783552	3160
#5	9	4	3	3	3	2	7700480	4120
#6	10	0	6	6	5	4	15843328	9900
#7	11	0	5	3	5	3	11714560	5907
#8	18	5	12	7	12	4	11288576	7028
#9	16	2	9	8	8	2	19791872	10188
#10	11	2	9	9	8	5	5701632	3296
#11	19	1	14	13	14	10	15056896	7821
#12	10	0	6	5	5	2	14090240	7214
Total	**145**	**27**	**90**	**77**	**85**	**53**	**118882304**	**65107**

To evaluate a different use-case, an additional experiment was conducted aimed at maximizing distance-to-vessels. For each electrode, both the SZ and entry-SZ were measured with Depth Map, and later, the Alternative Finder was run iteratively with increasing diameter of entry-SZ and SZ requirements (in steps of 1mm, favoring the entry-SZ over the SZ), until a maximum was found. Please note that when the diameter of the SZ is over 10 mm, it is presented as 10 mm in the graph, as that is the maximum diameter that can be measured with the Depth Map in the described configuration. In this additional experiment, every trajectory obtained enhanced avascular SZ values (Figure 4.9).
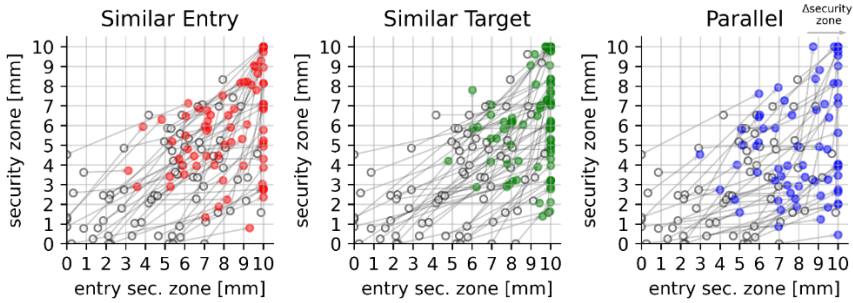
Figure 4.9 Dynamic optimization of entry-SZ and SZ. Every trajectory is enhanced in terms of an increase of its security zones, with a preference for the entry-SZ over the SZ. Preliminary trajectory security zones (empty white circle) are united to their final optimized trajectories (color depending on optimization strategy) with an arrow.

4.4 Discussion

SEEG is a complex procedure requiring collaboration from several clinical specialties. The presented work fits in the workflow right after the epileptologist has provided its initial trajectories, and it is aimed at aiding neurosurgeons, with tools to early detect and discard problematic trajectories and find alternative ones when required. The Alternative Finder tool is designed to adhere to different aspects of an initially planned trajectory. The reason we have not yet addressed the definition of that initial trajectory is that we have not found a practical way to that map seizure semiology (an important criterion for establishing the EZ localization hypothesis) into 3D space due to its non-image nature and complex symptom classification.

An experiment was presented to evaluate the search for the closest avascular trajectory given two fixed expected SZ values (usually the same for the whole plan). In the experiment, the user clicks and waits for the answer. Computation time is within acceptable values for an interactive tool, with response times well below one second. The presented method uses only hard constraints [105, 114], and it can early abort a search when no possible alternatives are found for one of the constraints (e.g., vessels at the entry), yielding response times as low as 8 ms for the parallel-alternatives computation.

As seen in Figure 4.8, the *similar entry* approach produces smaller displacements on the entry than on the target. The opposite happens in the *similar-target* approach, demonstrating adherence to the initial trajectory in different ways. From all cited research, only De Momi et al. [105] addressed the issue of adherence to the entry and the target points and provides a qualitative evaluation of the results. Our study introduces a quantitative evaluation of the adherence adding yet another adherence option with the parallel strategy, obtaining alternative trajectories with the same insertion angles.

In Figure 4.8 the histogram for parallel alternatives is identical for the entry and target point displacement, which was expected. This method may be used for parallel implantations [62, 119], and it offers similarities with the original SEEG carried out in the Sainte Anne Hospital, France [27]. The parallel search described in this work is too strict and does not consider trajectories whose angles deviate slightly that of the initial trajectory, and it will be the subject of future work.

Visualization of surgical risk in a cortical mesh is valid for procedures where only the tip of the trajectory is relevant (e.g., DBS, needle biopsy) but it would not be useful for plotting risks associated with a fixed entry and multiple target points. Our visualization shares similarities with the MIP approach presented by the Milan group [42], but offers some extra advantages. The Depth Map tool records depth along the trajectory which is used by the user interface to let the user interactively inspect the tri-planar view of the original image simply by clicking on the desired part of the 3D vessel. This visualization is more natural to the user's eye than MIP, as objects closer to the user's eye occlude distant ones. Lastly, our tool scans the whole length of the trajectory, instead of the first centimeter. Our visualization provides radial positioning of the risks with respect to the trajectory axis, which cannot be visualized in the distance graph widget provided within Epinav [47]. This in turn provides more precise depth information that could be very useful during the implantation. Both visualization widgets are complementary and will be the subject of future work.

A recent publication examines 8 different heuristics used by different tools to optimize SEEG [123], where the first one was the

maximizing distance from the vasculature. The second one was to avoid sulci (which we have tested using sulci information provided by Freesurfer [36]) but the main reason to do so is to avoid vessels, and we have opted to use DSA for that constraint. Furthermore, sulci avoidance conflicts with the next listed heuristic which is to maximize gray matter sampling. The drilling angle with the skull is another common heuristic, which our tool handles differently. Instead of providing the system with only a target point, we require an initial trajectory to be specified, and we guarantee that the trajectory does not deviate more than a certain angle.

The presented computations have the advantage of working directly with the original volumes, not requiring an intermediate mesh representation of the patient, although currently still require manual thresholding of the DSA. It can also be used with meshes, either with a distance map computation or directly projecting the mesh, in which case special care needs to be taken to prevent rendering of the inside of the mesh, which is empty and could return false negatives.

Another contribution of our method is that it is fully parametrizable, independently of the characteristics of the input datasets (e.g., cortical mesh resolution). This allows flexible configuration (search angle, number of trajectories to scan) through modification of specific parts of the rendering pipeline, as described in the Depth Map and Alternative Finder subsections.

When considering DSA imaging, finding avascular trajectories becomes more challenging than with a T1-weighted MRI scan with gadolinium enhancement, due to the increased number of vessels. DSA is an invasive technique with its own associated risks, and its benefits are under active investigation [124]. As discussed [41], visualization and assisted planning are highly dependent on vessel segmentation quality, which is an area of active research [125].

A pilot study has been conducted with clinicians from Hospital del Mar to evaluate the use of the described methods in a prospective setup, showing that the tool might be useful for early risk assessment. The tool has proven useful in finding avascular trajectories both from preliminary trajectories and for more definitive ones, where the algorithm performs very subtle modifications to the trajectories. The

most prevalent cause of false-positive alternatives has been incorrect vessel segmentation. Another undesired effect happened when the proposed alternative moved to a different brain gyrus. The described method has been integrated into the SYLVIUS stereotactic surgical planning platform. A patent has been filed for the Trajectory Finder method that searches for alternative trajectories. Future work will concentrate on exploring better segmentation of the DSA and other less invasive imaging modalities, computing electrode reports on tissue traversed, enhancing visualization and interaction, and providing preset avascular trajectory search within a certain brain region obtained from brain parcellations.

4.5   Conclusion

We have presented two automated tools that allow clinicians to examine and re-plan SEEG trajectories for avoiding risky structures while maximizing adherence with three possible adherence strategies, both performing at interactive speeds. A quantitative experiment has been conducted to measure the different re-planning strategies yield the expected adherence results. A graphical interface designed for trajectory evaluation in the clinical environment was implemented to allow the user to evaluate the tools. The presented tools work directly with volumetric images and can also be used with meshes. These tools provide early alarms and fast suggestions but do not replace the manual inspection of the trajectories, as they rely on the quality of the segmentation.

5 CONCLUSIONS

5.1 Summary of contributions

We have developed SYLVIUS, a software platform intended to facilitate and improve the complex workflow of epilepsy surgery providing pre and postoperative tools for electrode implantation and EZ resection. The software is installed in a compact head-tracking capable 3D platform (zSpace), which has been used to visualize complex anatomical structures such as vessels or segmented white matter tracts. Tools to visualize electrical information obtained from SEEG recordings, segment the postoperative data, import/export surgical plans from/to two robotic implantation systems, and analyze the tractography information with trajectories and contacts have also been developed and integrated into our surgical planning platform.

SYLVIUS has allowed combining digital subtraction angiography with the surgical plan based on T1-Gd, allowing the neurosurgery team to identify a higher number of vessel-intersecting trajectories. A study has been performed to investigate the number and magnitude of trajectory corrections performed after adding the digital subtraction angiography to the case.

In the context of automated surgical planning, we have created a tool that raises early alarms when trajectories traverse vascular structures which could be damaged, and another one to replan trajectories considering adherence to the epileptologist plan with three different strategies. These tools map the three-dimensional problem into the two-dimensional domain providing multiple computational benefits and allowing for the evaluation of a great number of alternatives.

The SYLVIUS platform has been used in the clinical routine at Hospital del Mar, Barcelona, to modify trajectories in nineteen SEEG implantation cases, without any reported complication.

5.2 List of contributions

In the following list, we enumerate the main scientific and industrial contributions:

Peer-reviewed papers in international journals:

A. Higueras-Esteban, I. Delgado-Martínez, L. Serrano, A. Principe, C.P. Enriquez, M.A.G. Ballester, R. Rocamora, G. Conesa, L. Serra, **SYLVIUS: A multimodal and multidisciplinary platform for epilepsy surgery**, *Computer Methods and Programs in Biomedicine 203 (2021) 106042. https://doi.org/https://doi.org/10.1016/j.cmpb.2021.106042.*

I. Delgado-Martínez, L. Serrano, A. Higueras-Esteban, E. Vivas, R. Rocamora, M.A. González Ballester, L. Serra, G. Conesa, On the Use of Digital Subtraction Angiography in Stereoelectroencephalography Surgical Planning to Prevent Collisions with Vessels, World Neurosurgery 147 (2021) 47–56. https://doi.org/10.1016/j.wneu.2020.11.103.

A. Higueras-Esteban, I. Delgado-Martínez, L. Serrano, N. Infante-Santos, A. Narváez-Martínez, A. Principe, R. Rocamora, G. Conesa, L. Serra, M.A. González Ballester, **Projection-based collision detection algorithm for Stereoelectroencephalography (SEEG) electrode risk assessment and re-planning,** *Submitted(2021).*

Peer-reviewed abstracts for conference proceedings:

A. Higueras-Esteban, J. Ojeda, I. Delgado-Martínez, C.P. Enríquez, L. Serrano, A. Principe, M.A. González Ballester, R. Rocamora, L. Serra, G. Conesa, **Automatic segmentation of deep brain electrodes used in stereotactic electroencephalography (SEEG)**, *International Journal of Computer Assisted Radiology and Surgery 13 (2018) 79–80. https://doi.org/10.1007/s11548-018-1766-y.*

A. Higueras-Esteban, I. Delgado-Martínez, L. Serrano, G. Conesa, M.A. González Ballester, L. Serra, **Volume rendering depth mapping for fast vessel identification during intracranial deep electrode planning**, *International Journal of Computer Assisted Radiology and Surgery (Suppl 1). 14 (2019) 150–151. https://doi.org/10.1007/s11548-019-01969-3.*

A. Higueras-Esteban, I. Delgado-Martínez, L. Serrano, A. Principe, M.A. González Ballester, R. Rocamora, L. Serra, G. Conesa, **Diffusion Weighted Imaging (DWI) tractography filtering tools for for Stereotactic Electro-Encephalography (SEEG)**, *International Journal of Computer Assisted Radiology and Surgery (Suppl 1). 15 (2020) 90-91. https://doi.org/10.1007/s11548-020-02171-6.*

Patents (Europe and US):

> *Higueras Esteban A., Serra L., Conesa G., Delgado-Martínez I., González Ballester M.A. Computer implemented method, a system and computer programs for computing simultaneous rectilinear paths using medical images.* **US Patent** *application no. 16/902912, 16 June 2020*

> *Higueras A., Serra L., Conesa G., Delgado-Martínez I., González Ballester M.A. A computer implemented method, a system and computer programs for computing simultaneous rectilinear paths using medical images.* **European Patent** *application no. EP19382502, 17 June 2019.*

Besides industrial property rights and the scientific publications, within the scope of this thesis a software planning platform has been developed and has been deployed to our reference center, where it is being used routinely in conjunction with the robot planning software.

5.3 Future work

5.3.1 Other stereotactic interventions

There are other stereotactic neurosurgical procedures that share many commonalities with SEEG interventions. Besides epilepsy, SYLVIUS has been used for other stereotactic procedures in neurosurgery. SYLVIUS has been used for planning of tumor treatment using laser interstitial thermal therapy (LITT)[1]. This kind of intervention can be used among other things to perform the final step of epilepsy surgery to perform the ablation. Figure 5.1 shows a hamartoma ablation case that was analyzed within the SYLVIUS platform. Another interesting line of research is deep brain stimulation [50], which opens the door to a broad range of functional neurosurgeries.
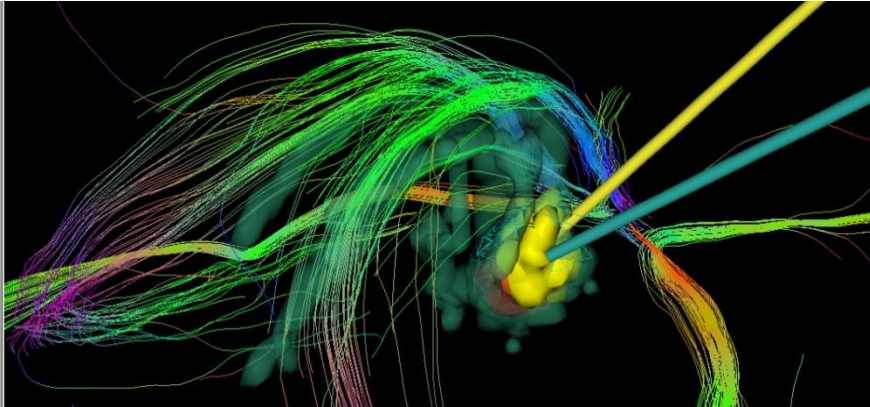
Although stereotactic procedures share many commonalities, each procedure has its own requirements, mainly due to the delivery system used. For LITT, it is vital to control the temperature around the laser probe. One possible line of work is the combination of magnetic resonance thermographic maps with the anatomical and DWI tractography information in real-time procedure monitoring. For DBS, an in-depth investigation of the published literature regarding the area of tissue activated would be an important task.

5.3.2 Implantation platforms

A limitation of the current work is that it relies on a limited number of implantation platforms to perform the surgery (ROSA® and Renishaw®). A future line of development could be the integration of other implantation platforms. Some work has been devoted to the inclusion of stereotactic frames to increase the number of hospitals that could use the platform. In particular, interoperability with the Micromar® stereotactic frame's coordinate system has been tested (Figure 5.2), but this frame can be used in different positions, resulting in different final coordinates, and integrating that into SYLVIUS could be another feature to develop.
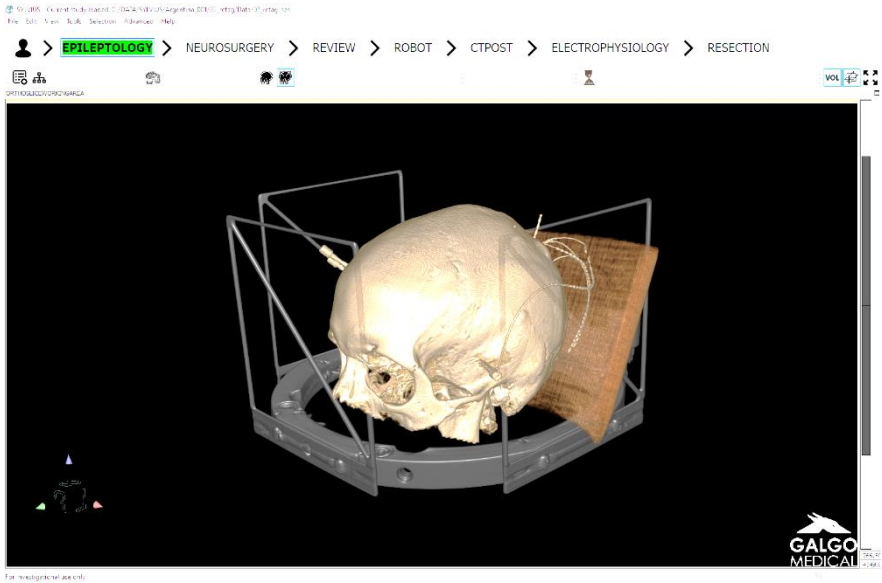
Figure 5.2 Micromar stereotactic frame

One possible research goal would be to consider the three-dimensional representation of the stereotactic frame for surgical planning. Sometimes during the implantation, the stereotactic frame blocks certain planned entry points, and that situation could be prevented with the mentioned feature. Besides, a platform like zSpace® could help in the creation of an intuitive interaction to locate the stereotactic frame model with respect to preoperative data.

Another exciting line of work could be the use of 3D-printed robotics to tackle the specific goal of stereotactic surgery. Some promising work has been done here at the UPF with BCN3D MOVEO, an open-source robotic arm developed by BCN3D and the Departament d'Ensenyament de la Generalitat de Catalunya. Thanks to its 3D printed and open-source design, the robot arm tooltip could be specifically designed to suit different steps of the stereotactic procedure.
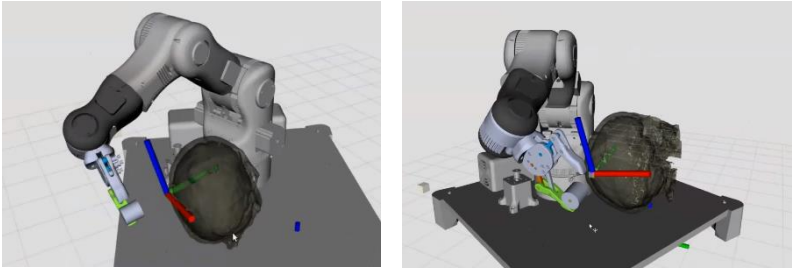
Figure 5.3 BCN3D MOVEO 3D printed robot arm simulating implantation of SYLVIUS exported case. Courtesy of Mario Ceresa and Gerard Marturià

5.3.3 Seizure propagation analysis

The combination of diverse patient data has allowed for the visualization of brain connectivity together with detailed intracranial electrical measurements and a variety of three-dimensional anatomical images. One possible future research line could be the visualization and analysis of seizure propagation. This may contribute to the future understanding of epileptic networks, allowing for future interventions to be designed for disconnection of the seizure propagation path.
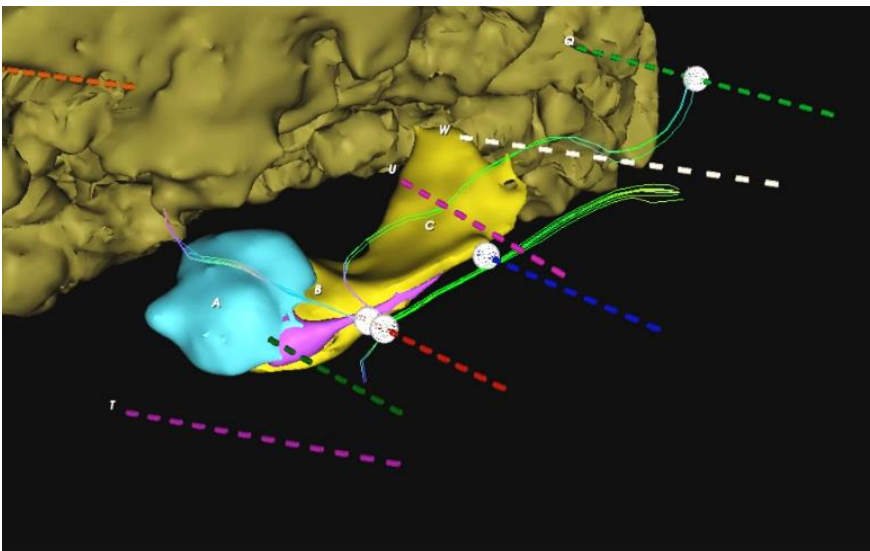
Figure 5.4 SEEG-Electrome: Four electrical regions defined by electric contacts I bipolar configuration connected via DWI tracts. White spheres are located at the intersection of two consecutive contacts. Tractography was computed with the Dextroscope®.

The SEEG-electrome tool (Figure 2.12, Figure 5.4) could be used to locate and analyze the relationship between the distant electrical readings of areas connected via DWI paths. A possible start might be to analyze different power bands of connected regions. Another line of research could be the evaluation and validation of different brain tractography algorithms using electrical measurements.

5.3.4 Automatic trajectory planning

Regarding automated trajectory planning, one possible route would be to make more extensive use of the depth information retrieved by the described method. It might be possible to use the depth map to decide the next position in which to search for possible avascular paths.

In the short term, some future work might be devoted to combining our method with other ones described in the literature in terms of computation, trajectory initialization, and visualization.

Another issue is the addition of other surgical constraints to the automatic trajectory planning algorithm. Some preliminary work was performed to import sulci information from Freesurfer[36], as seen in Figure 5.5. Future work could be to allow the user to decide if brain sulci should be treated as no-go zones.
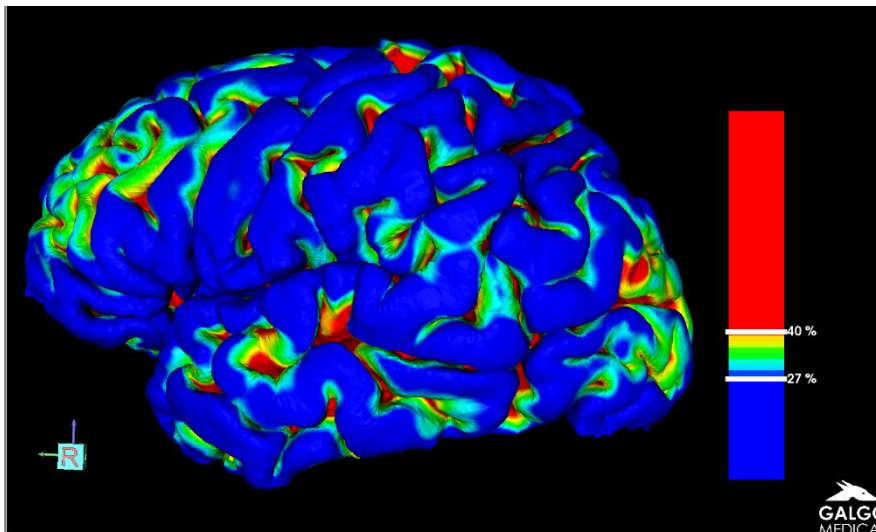
Figure 5.5 Freesurfer sulci information imported. This work was carried out by Gerard Manturià during his in-company training at Galgo Medical S.L.

A possible line of research which could potentially have a big impact could be to obtain a vessel segmentation from other imaging modality with fewer risks associated than DSA, but retaining similar segmentation quality.

5.3.5 Visualization and interaction

Another important line of work could be concerned with the integration of a more powerful multimodal volume renderer into the surgical planning platform to enhance its visualization and interaction capabilities. A screenshot from an internally developed advanced multimodal 3D-stereo capable volume renderer can be seen in Figure 5.6. In the picture, a zSpace® laptop is depicted, which provides less computational power but with a much more compact design. Creating a fluid 3D-stereo multimodal experience, fully integrated with SYLVIUS, could be an interesting future line of development.

Figure 5.6 Multimodal Volume Rendered in zSpace® laptop. Courtesy of Galgo Medical S.L.

Integrating the risk visualization tool provided Epinav™ into SYLVIUS could be another area for future work.

5.3.6 Clinical evaluation

A limitation of the evaluation of the presented tools is that it has not been performed by clinicians from other centers with expertise in

epilepsy surgery. Multiple collaborations with other hospitals have already been established for a possible future evaluation of the platform, and the development of a modules for working with stereotactic frames to increase clinical adoption. We believe that the prospective clinical evaluation of SYLVIUS, and particularly of the Depth Map and Alternative Finder tools described in Chapter 4, would prove the usefulness of the technologies developed in this thesis.

Bibliography

[1]   Dorfer, C.; Rydenhag, B.; Baltuch, G.; Buch, V.; Blount, J.; Bollo, R.; Gerrard, J.; Nilsson, D.; Roessler, K.; Rutka, J.; Sharan, A.; Spencer, D.; Cukiert, A. (2020). How technology is driving the landscape of epilepsy surgery, *Epilepsia*, Vol. 61, No. 5, 841–855. doi:10.1111/epi.16489

[2]   Ntoukas, V.; Müller, A. (2010). Minimally invasive approach versus traditional open approach for one level posterior lumbar interbody fusion, *Minimally Invasive Neurosurgery*, Vol. 53, No. 01, 21–24

[3]   Al-Khouja, L. T.; Baron, E. M.; Johnson, J. P.; Kim, T. T.; Drazin, D. (2014). Cost-effectiveness analysis in minimally invasive spine surgery, *Neurosurgical Focus*, Vol. 36, No. June, 1–9. doi:https://doi.org/10.3171/2014.4.FOCUS1449

[4]   Galloway, R. L.; Maciunas, R. J. (1990). Stereotactic neurosurgery, *Critical Reviews in Biomedical Engineering*, Vol. 18, No. 3, 181–205

[5]   Navkar, N. V.; Tsekos, N. V.; Stafford, J. R.; Weinberg, J. S.; Deng, Z. (2010). Visualization and planning of neurosurgical interventions with straight access, *Lecture Notes in Computer Science (Including Subseries Lecture Notes in Artificial Intelligence and Lecture Notes in Bioinformatics)*, Vol. 6135 LNCS, 1–11. doi:10.1007/978-3-642-13711-2_1

[6]   Horsley, V.; Clarke, R.; Mussen, A.; Mussen, D. (2009). Early history of the stereotactic apparatus in neurosurgery, *Neurosurgical Focus*, Vol. 27, No. 3, 1–5. doi:10.3171/2009.7.FOCUS09118

[7]   Quadri, S. A.; Waqas, M.; Khan, I.; Khan, M. A.; Suriya, S. S.; Farooqui, M.; Fiani, B. (2018). High-intensity focused ultrasound: Past, present, and future in neurosurgery, *Neurosurgical Focus*, Vol. 44, No. 2, 1–9. doi:10.3171/2017.11.FOCUS17610

[8]   Barnett, G. H.; Linskey, M. E.; Adler, J. R.; Cozzens, J. W.; Friedman, W. A.; Heilbrun, M. P.; Lunsford, L. D.; Schulder, M.; Sloan, A. E.; title =. (2007). Stereotactic radiosurgery—an organized neurosurgery-sanctioned definition, *Journal of*

Neurosurgery, No. 106. doi:https://doi.org/10.3171/jns.2007.106.1.1

[9]   Halasz, L. M.; Rockhill, J. K. (2013). Stereotactic radiosurgery and stereotactic radiotherapy for brain metastases, *Surgical Neurology International SNI:*, Vol. 4, 185–191. doi:10.4103/2152-7806.111295

[10] Nowell, M.; Rodionov, R.; Zombori, G.; Sparks, R.; Winston, G.; Kinghorn, J.; Diehl, B.; Wehner, T.; Miserocchi, A.; McEvoy, A. W.; Ourselin, S.; Duncan, J. (2015). Utility of 3D multimodality imaging in the implantation of intracranial electrodes in epilepsy, *Epilepsia*, Vol. 56, No. 3, 403–413. doi:10.1111/epi.12924

[11] Panigrahi, M.; Jayalakshmi, S. (2008). Presurgical evaluation of epilepsy, *Journal of Pediatric Neurosciences*, Vol. 3, No. 1, 74. doi:10.4103/1817-1745.40593

[12] Delgado-Martínez, I.; Serra, L.; Rocamora, R.; Conesa, G. (2019). Multidisciplinary planning of deep electrode implantation, G. H. Baltuch; A. Cukiert (Eds.), *Operative Techniques in Epilepsy Surgery* (2nd ed.), Thieme Medical Publishers, Inc., 1–14

[13] Fisher, R. S.; Acevedo, C.; Arzimanoglou, A.; Bogacz, A.; Cross, J. H.; Elger, C. E.; Engel, J.; Forsgren, L.; French, J. A.; Glynn, M.; Hesdorffer, D. C.; Lee, B. I.; Mathern, G. W.; Mosh??, S. L.; Perucca, E.; Scheffer, I. E.; Tomson, T.; Watanabe, M.; Wiebe, S. (2014). ILAE Official Report: A practical clinical definition of epilepsy, *Epilepsia*, Vol. 55, No. 4, 475–482. doi:10.1111/epi.12550

[14] Scheffer, I. E.; Berkovic, S.; Capovilla, G.; Connolly, M. B.; French, J.; Guilhoto, L.; Hirsch, E.; Jain, S.; Mathern, G. W.; Moshé, S. L.; Nordli, D. R.; Perucca, E.; Tomson, T.; Wiebe, S.; Zhang, Y. H.; Zuberi, S. M. (2017). ILAE classification of the epilepsies: Position paper of the ILAE Commission for Classification and Terminology, *Epilepsia*, Vol. 58, No. 4, 512–521. doi:10.1111/epi.13709

[15] Laxer, K. D.; Trinka, E.; Hirsch, L. J.; Cendes, F.; Langfitt, J.; Delanty, N.; Resnick, T.; Benbadis, S. R. (2014). The consequences of refractory epilepsy and its treatment, *Epilepsy and Behavior*, Vol. 37, 59–70.

doi:10.1016/j.yebeh.2014.05.031

[16] Guglielmi, G. (2002). Bromide, the first effective antiepileptic agent, *AJNR. American Journal of Neuroradiology*, Vol. 23, No. 2, 342. doi:10.1176/ajp.120.8.817

[17] Errante, L. D.; Williamson, A.; Spencer, D. D.; Petroff, O. A. C. (2002). Gabapentin and vigabatrin increase GABA in the human neocortical slice, *Epilepsy Research*, Vol. 49, No. 3, 203–210. doi:10.1016/S0920-1211(02)00034-7

[18] Abou-al-shaar, H.; Brock, A. A.; Kundu, B.; Englot, D. J.; John, D.; City, S. L.; States, U.; States, U. (2018). Increased nationwide use of stereoencephalography for intracranial epilepsy electroencephalography recordings, *Journal of Clinical Neuroscience*, 132–134. doi:10.1016/j.jocn.2018.04.064.Increased

[19] Kwan, P.; Brodie, M. J. (2002). Early Identification of Refractory Epilepsy, *New England Journal of Medicine*, Vol. 342, No. 5, 314–319. doi:10.1056/nejm200002033420503

[20] Jehi, L. (2018). The epileptogenic zone: Concept and definition, *Epilepsy Currents*, Vol. 18, No. 1, 12–16. doi:10.5698/1535-7597.18.1.12

[21] Munari, C.; Bancaud, J. (1985). The role of stereo-EEG in the evaluation of partial epileptic seizures, *The Epilepsies. London: Butterworths*, 267–306

[22] Talairach, J.; Bancaud, J. (1966). Lesion," irritative" zone and epileptogenic focus, *Stereotactic and Functional Neurosurgery*, Vol. 27, Nos. 1–3, 91–94

[23] Lüders, H. O.; Najm, I.; Nair, D.; Widdess-Walsh, P.; Bingman, W. (2006). The epileptogenic zone: General principles, *Epileptic Disorders*, Vol. 8, No. SUPPL. 2, 1–9. doi:10.3109/9780203091708-107

[24] Rosenow, F.; Lüders, H. (2001). Presurgical evaluation of epilepsy, *Brain*, Oxford University Press, 1683–1700. doi:10.1093/brain/124.9.1683

[25] Cardinale, F.; Rizzi, M.; Vignati, E.; Cossu, M.; Castana, L.; d'Orio, P.; Revay, M.; Costanza, M. Della; Tassi, L.; Mai, R.; Sartori, I.; Nobili, L.; Gozzo, F.; Pelliccia, V.; Mariani, V.; Russo, G. Lo; Francione, S. (2019).

Stereoelectroencephalography: Retrospective analysis of 742 procedures in a single centre, *Brain*, Vol. 142, No. 9, 2688–2704. doi:10.1093/brain/awz196

[26] Gonzalez-Martinez, J.; Mullin, J.; Vadera, S.; Bulacio, J.; Hughes, G.; Jones, S.; Enatsu, R.; Najm, I. (2014). Stereotactic placement of depth electrodes in medically intractable epilepsy., *Journal of Neurosurgery*, Vol. 120, No. 3, 639–44. doi:10.3171/2013.11.JNS13635

[27] Cardinale, F.; Casaceli, G.; Raneri, F.; Miller, J.; Lo Russo, G. (2016). Implantation of Stereoelectroencephalography Electrodes: A Systematic Review, *Journal of Clinical Neurophysiology*, Vol. 33, No. 6, 490–502. doi:10.1097/WNP.0000000000000249

[28] Nowell, M.; Sparks, R.; Zombori, G.; Miserocchi, A.; Rodionov, R.; Diehl, B.; Wehner, T.; Baio, G.; Trevisi, G.; Tisdall, M.; Ourselin, S.; Mcevoy, A. W.; Duncan, J. (2015). Comparison of computer-assisted planning and manual planning for depth electrode implantations in epilepsy, *Journal of Neurosurgery*, 1–3. doi:10.3171/2015.6.JNS15487.

[29] Wellmer, J.; Parpaley, Y.; Rampp, S.; Popkirov, S.; Kugel, H.; Aydin, Ü.; Wolters, C. H.; von Lehe, M.; Voges, J. (2016). Lesion guided stereotactic radiofrequency thermocoagulation for palliative, in selected cases curative epilepsy surgery, *Epilepsy Research*, Vol. 121, 39–46. doi:10.1016/j.eplepsyres.2016.01.005

[30] Fritzsche, K. H.; Neher, P. F.; Reicht, I.; van Bruggen, T.; Goch, C.; Reisert, M.; Nolden, M.; Zelzer, S.; Meinzer, H. P.; Stieltjes, B. (2012). MITK diffusion imaging, *Methods of Information in Medicine*, Vol. 51, No. 5, 441–448. doi:10.3414/ME11-02-0031

[31] Dell'Acqua, F.; Scifo, P.; Rizzo, G.; Catani, M.; Simmons, A.; Scotti, G.; Fazio, F. (2010). A modified damped Richardson-Lucy algorithm to reduce isotropic background effects in spherical deconvolution, *NeuroImage*, Vol. 49, No. 2, 1446–1458. doi:10.1016/j.neuroimage.2009.09.033

[32] Tournier, J. D.; Calamante, F.; Connelly, A. (2012). MRtrix: Diffusion tractography in crossing fiber regions, *International Journal of Imaging Systems and Technology*, Vol. 22, No. 1,

53–66. doi:10.1002/ima.22005

[33] Huppertz, H. J.; Wellmer, J.; Staack, A. M.; Altenmüller, D. M.; Urbach, H.; Kröll, J. (2008). Voxel-based 3D MRI analysis helps to detect subtle forms of subcortical band heterotopia, *Epilepsia*, Vol. 49, No. 5, 772–785. doi:10.1111/j.1528-1167.2007.01436.x

[34] Smith, S. M.; Jenkinson, M.; Woolrich, M. W.; Beckmann, C. F.; Behrens, T. E. J.; Johansen-Berg, H.; Bannister, P. R.; De Luca, M.; Drobnjak, I.; Flitney, D. E.; Niazy, R. K.; Saunders, J.; Vickers, J.; Zhang, Y.; De Stefano, N.; Brady, J. M.; Matthews, P. M. (2004). Advances in functional and structural MR image analysis and implementation as FSL, *NeuroImage*, Vol. 23, No. SUPPL. 1, 208–219. doi:10.1016/j.neuroimage.2004.07.051

[35] Jatoi, M. A.; Kamel, N.; Malik, A. S.; Faye, I.; Begum, T. (2014). A survey of methods used for source localization using EEG signals, *Biomedical Signal Processing and Control*, Vol. 11, No. 1, 42–52. doi:10.1016/j.bspc.2014.01.009

[36] Fischl, B. (2012). FreeSurfer, *NeuroImage*, Vol. 62, No. 2, 774–781. doi:10.1016/j.neuroimage.2012.01.021

[37] Cardinale, F.; Cossu, M.; Castana, L.; Casaceli, G.; Schiariti, M. P.; Miserocchi, A.; Fuschillo, D.; Moscato, A.; Caborni, C.; Arnulfo, G.; Lo Russo, G. (2013). Stereoelectroencephalography: Surgical methodology, safety, and stereotactic application accuracy in 500 procedures, *Neurosurgery*, Vol. 72, No. 3, 353–366. doi:10.1227/NEU.0b013e31827d1161

[38] Cardinale, F.; Rizzi, M.; D'Orio, P.; Casaceli, G.; Arnulfo, G.; Narizzano, M.; Scorza, D.; De Momi, E.; Nichelatti, M.; Redaelli, D.; Sberna, M.; Moscato, A.; Castana, L. (2017). A new tool for touch-free patient registration for robot-assisted intracranial surgery: Application accuracy from a phantom study and a retrospective surgical series, *Neurosurgical Focus*, Vol. 42, No. 5, 1–7. doi:10.3171/2017.2.FOCUS16539

[39] Cardinale, F.; Pero, G.; Quilici, L.; Piano, M.; Colombo, P.; Moscato, A.; Castana, L.; Casaceli, G.; Fuschillo, D.; Gennari, L.; Cenzato, M.; Lo Russo, G.; Cossu, M. (2015). Cerebral Angiography for Multimodal Surgical Planning in Epilepsy

Surgery: Description of a New Three-Dimensional Technique and Literature Review, *World Neurosurgery*, Vol. 84, No. 2, 358–367. doi:10.1016/j.wneu.2015.03.028

[40] Caborni, C.; De Momi, E.; Antiga, L.; Hammoud, A.; Ferrigno, G.; Cardinale, F. (2012). Automatic trajectory planning in Stereo-electroencephalography image guided neurosurgery, *International Journal of Computer Assisted Radiology and Surgery*, Vol. 7, No. Suppl 1, S126–S127. doi:10.13140/2.1.4564.4806

[41] De Momi, E.; Caborni, C.; Cardinale, F.; Castana, L.; Casaceli, G.; Cossu, M.; Antiga, L.; Ferrigno, G. (2013). Automatic Trajectory Planner for StereoElectroEncephaloGraphy Procedures: A Retrospective Study, *IEEE Transactions on Biomedical Engineering*, Vol. 60, No. 4, 986–993. doi:10.1109/TBME.2012.2231681

[42] Scorza, D.; Moccia, S.; De Luca, G.; Plaino, L.; Cardinale, F.; Mattos, L. S.; Kabongo, L.; De Momi, E. (2017). Safe electrode trajectory planning in SEEG via MIP-based vessel segmentation, *Proc. SPIE 10135, Medical Imaging 2017: Image-Guided Procedures, Robotic Interventions, and Modeling*, Vol. 10135, No. i, 101352C-101352C8. doi:10.1117/12.2254474

[43] Narizzano, M.; Arnulfo, G.; Ricci, S.; Toselli, B.; Tisdall, M.; Canessa, A.; Fato, M. M.; Cardinale, F. (2017). SEEG assistant: a 3DSlicer extension to support epilepsy surgery, *BMC Bioinformatics*, Vol. 18, No. 1, 124. doi:10.1186/s12859-017-1545-8

[44] Nowell, M.; Sparks, R.; Zombori, G.; Miserocchi, A.; Rodionov, R.; Diehl, B.; Wehner, T.; Baio, G.; Trevisi, G.; Tisdall, M.; Ourselin, S.; McEvoy, A. W.; Duncan, J. (2016). Comparison of computer-assisted planning and manual planning for depth electrode implantations in epilepsy, *Journal of Neurosurgery*, Vol. 124, No. 6, 1820–1828. doi:10.3171/2015.6.JNS15487

[45] Vakharia, V. N.; Sparks, R.; Miserocchi, A.; Vos, S. B.; O'Keeffe, A.; Rodionov, R.; McEvoy, A. W.; Ourselin, S.; Duncan, J. S. (2019). Computer-Assisted Planning for Stereoelectroencephalography (SEEG), *Neurotherapeutics*,

Vol. 16, No. 4, 1183–1197. doi:10.1007/s13311-019-00774-9

[46]   Nowell, M.; Rodionov, R.; Zombori, G.; Sparks, R.; Rizzi, M.; Ourselin, S.; Miserocchi, A.; McEvoy, A.; Duncan, J. (2016). A Pipeline for 3D Multimodality Image Integration and Computer-assisted Planning in Epilepsy Surgery, *Journal of Visualized Experiments*, No. 111, 1–10. doi:10.3791/53450

[47]   Zombori, G.; Rodionov, R.; Nowell, M.; Zuluaga, M. A.; Clarkson, M. J.; Micallef, C.; Diehl, B.; Wehner, T.; Miserochi, A.; McEvoy, A. W.; Duncan, J. S.; Ourselin, S. (2014). A computer assisted planning system for the placement of sEEG electrodes in the treatment of epilepsy, *In: Stoyanov D., Collins D.L., Sakuma I., Abolmaesumi P., Jannin P. (Eds) Information Processing in Computer-Assisted Interventions. IPCAI 2014. Lecture Notes in Computer Science.*, Vol. 8498, 118–127. doi:10.1007/978-3-319-07521-1_13

[48]   Drouin, S.; Kochanowska, A.; Kersten-Oertel, M.; Gerard, I. J.; Zelmann, R.; De Nigris, D.; Bériault, S.; Arbel, T.; Sirhan, D.; Sadikot, A. F.; Hall, J. A.; Sinclair, D. S.; Petrecca, K.; DelMaestro, R. F.; Collins, D. L. (2017). IBIS: an OR ready open-source platform for image-guided neurosurgery, *International Journal of Computer Assisted Radiology and Surgery*, Vol. 12, No. 3, 363–378. doi:10.1007/s11548-016-1478-0

[49]   Zelmann, R.; Beriault, S.; Mok, K.; Haegelen, C.; Hall, J.; Pike, G. B.; Olivier, A.; Collins, D. L. (2016). Automatic Optimization of Depth Electrode Trajectory Planning, *Clinical Image-Based Procedures. Translational Research in Medical Imaging.*, Vol. 9958, 99–107. doi:10.1007/978-3-319-46472-5

[50]   Bériault, S.; Subaie, F. Al; Collins, D. L.; Sadikot, A. F.; Pike, G. B. (2012). A multi-modal approach to computer-assisted deep brain stimulation trajectory planning, *International Journal of Computer Assisted Radiology and Surgery*, Vol. 7, No. 5, 687–704. doi:10.1007/s11548-012-0768-4

[51]   Miocinovic, S.; Noecker, A. M.; Maks, C. B.; Butson, C. R.; McIntyre, C. C. (2007). Cicerone: Stereotactic neurophysiological recording and deep brain stimulation

electrode placement software system, *Acta Neurochirurgica, Supplementum*, Vol. 97, No. 97 PART 2, 561–567. doi:10.1007/978-3-211-33081-4_65

[52] D'Haese, P. F.; Pallavaram, S.; Li, R.; Remple, M. S.; Kao, C.; Neimat, J. S.; Konrad, P. E.; Dawant, B. M. (2012). CranialVault and its CRAVE tools: A clinical computer assistance system for deep brain stimulation (DBS) therapy, *Medical Image Analysis*, Vol. 16, No. 3, 744–753. doi:10.1016/j.media.2010.07.009

[53] Essert, C.; Haegelen, C.; Jannin, P. (2010). Automatic computation of electrodes trajectory for deep brain stimulation, *In International Workshop on Medical Imaging and Virtual Reality*, Vol. 6326 LNCS, 149–158. doi:10.1007/978-3-642-15699-1_16

[54] Kockro, R. A.; Tsai, Y. T.; Ng, I.; Hwang, P.; Zhu, C.; Agusanto, K.; Hong, L. X.; Serra, L. (2009). DEX-Ray: Augmented reality neurosurgical navigation with a handheld video probe, *Neurosurgery*, Vol. 65, No. 4, 795–807. doi:10.1227/01.NEU.0000349918.36700.1C

[55] Kockro, R. A.; Serra, L.; Yeo, T. T.; Chan, C.; Sitoh, Y. Y.; Chua, G. G.; Lee, E.; Lee, Y. H.; Ng, H.; Nowinski, W. L. (2000). Planning and simulation of neurosurgery in a virtual reality environment, *Neurosurgery*, Vol. 46, No. 1, 118–137. doi:10.1093/neurosurgery/46.1.118

[56] Shamir, R. R.; Horn, M.; Blum, T.; Mehrkens, J.; Shoshan, Y.; Joskowicz, L.; Navab, N. (2011). Trajectory planning with augmented reality for improved risk assessment in image-guided keyhole neurosurgery, *IEEE International Symposium on Biomedical Imaging: From Nano to Macro*, 1873–1876. doi:10.1109/ISBI.2011.5872773

[57] Aganj, I.; Yeo, B. T. T.; Sabuncu, M. R.; Fischl, B. (2013). On removing interpolation and resampling artifacts in rigid image registration, *IEEE Transactions on Image Processing*, Vol. 22, No. 2, 816–827. doi:10.1109/TIP.2012.2224356

[58] Wang, R.; Benner, T.; Sorensen, A. G.; Wedeen, V. J. (2007). Diffusion Toolkit : A Software Package for Diffusion Imaging Data Processing and Tractography, *Proc. Intl. Soc. Mag. Reson. Med.*, Vol. 15, 3720

[59] Stein, D.; Fritzsche, K. H.; Nolden, M.; Meinzer, H. P.; Wolf, I. (2010). The extensible open-source rigid and affine image registration module of the Medical Imaging Interaction Toolkit (MITK), *Computer Methods and Programs in Biomedicine*, Vol. 100, No. 1, 79–86. doi:10.1016/j.cmpb.2010.02.008

[60] Higueras-Esteban, A.; Delgado-Martínez, I.; Serrano, L.; Conesa, G.; González Ballester, M. A.; Serra, L. (2019). Volume rendering depth mapping for fast vessel identification during intracranial deep electrode planning, *International Journal of Computer Assisted Radiology and Surgery (Suppl 1)*, Vol. 14, No. June, 150–151. doi:10.1007/s11548-019-01969-3

[61] Arnulfo, G.; Narizzano, M.; Cardinale, F.; Fato, M. M.; Palva, J. M. (2015). Automatic segmentation of deep intracerebral electrodes in computed tomography scans., *BMC Bioinformatics*, Vol. 16, No. 1, 12–99. doi:10.1186/s12859-015-0511-6

[62] Medina Villalon, S.; Paz, R.; Roehri, N.; Lagarde, S.; Pizzo, F.; Colombet, B.; Bartolomei, F.; Carron, R.; Bénar, C. G. (2018). EpiTools, A software suite for presurgical brain mapping in epilepsy: Intracerebral EEG, *Journal of Neuroscience Methods*, Vol. 303, 7–15. doi:10.1016/j.jneumeth.2018.03.018

[63] Higueras-Esteban, A.; Ojeda, J.; Delgado-Martínez, I.; Enríquez, C. P.; Serrano, L.; Principe, A.; González Ballester, M. A.; Rocamora, R.; Serra, L.; Conesa, G. (2018). Automatic segmentation of deep brain electrodes used in stereotactic electroencephalography (SEEG), *International Journal of Computer Assisted Radiology and Surgery*, Vol. 13, 79–80. doi:10.1007/s11548-018-1766-y

[64] Higueras-Esteban, A.; Delgado-Martínez, I.; Serrano, L.; Principe, A.; González Ballester, M. A.; Rocamora, R.; Serra, L.; Conesa, G. (2020). Diffusion Weighted Imaging (DWI) tractography filtering tools for for Stereotactic Electro-Encephalography (SEEG), *International Journal of Computer Assisted Radiology and Surgery*, Vol. 15, 90–91. doi:10.1007/s11548-020-02171-6

[65] Li, A.; Mueller, K.; Ernst, T. (2004). Methods for efficient, high quality volume resampling in the frequency domain, *IEEE Visualization 2004 - Proceedings, VIS 2004*, 3–10. doi:10.1109/visual.2004.70

[66] Tandon, N.; Tong, B. A.; Friedman, E. R.; Johnson, J. A.; Von Allmen, G.; Thomas, M. S.; Hope, O. A.; Kalamangalam, G. P.; Slater, J. D.; Thompson, S. A. (2019). Analysis of Morbidity and Outcomes Associated With Use of Subdural Grids vs Stereoelectroencephalography in Patients With Intractable Epilepsy, *JAMA NEUROLOGY*, Vol. 76, No. 6, 672–681. doi:10.1001/jamaneurol.2019.0098

[67] Katz, J. S.; Abel, T. J. (2019). Stereoelectroencephalography Versus Subdural Electrodes for Localization of the Epileptogenic Zone: What Is the Evidence?, *Neurotherapeutics : The Journal of the American Society for Experimental NeuroTherapeutics*, Vol. 16, No. 1, 59–66. doi:10.1007/s13311-018-00703-2

[68] Mullin, J. P.; Shriver, M.; Alomar, S.; Najm, I.; Bulacio, J.; Chauvel, P.; Gonzalez-Martinez, J. (2016). Is SEEG safe? A systematic review and meta-analysis of stereo-electroencephalography-related complications, *Epilepsia*, Vol. 57, No. 3, 386–401. doi:10.1111/epi.13298

[69] McGovern, R. A.; Ruggieri, P.; Bulacio, J.; Najm, I.; Bingaman, W. E.; Gonzalez-Martinez, J. A. (2019). Risk analysis of hemorrhage in stereo-electroencephalography procedures., *Epilepsia*, Vol. 60, No. 3, 571–580. doi:10.1111/epi.14668

[70] Centeno, R. S.; Yacubian, E. M. T.; Caboclo, L. O. S. F.; Júnior, H. C.; Cavalheiro, S. (2011). Intracranial depth electrodes implantation in the era of image-guided surgery., *Arquivos de Neuro-Psiquiatria*, Vol. 69, No. July 2010, 693–698. doi:10.1590/S0004-282X2011000500022

[71] Abhinav, K.; Prakash, S.; Sandeman, D. R. (2013). Use of robot-guided stereotactic placement of intracerebral electrodes for investigation of focal epilepsy: Initial experience in the UK, *British Journal of Neurosurgery*, Vol. 27, No. 5, 704–705. doi:10.3109/02688697.2013.798859

[72] van der Loo, L. E.; Schijns, O. E. M. G.; Hoogland, G.; Colon,

A. J.; Wagner, G. L.; Dings, J. T. A.; Kubben, P. L. (2017). Methodology, outcome, safety and in vivo accuracy in traditional frame-based stereoelectroencephalography, *Acta Neurochirurgica*, Vol. 159, No. 9, 1733–1746. doi:10.1007/s00701-017-3242-9

[73] Rogosnitzky, M.; Branch, S. (2016). Gadolinium-based contrast agent toxicity: a review of known and proposed mechanisms., *Biometals : An International Journal on the Role of Metal Ions in Biology, Biochemistry, and Medicine*, Vol. 29, No. 3, 365–76. doi:10.1007/s10534-016-9931-7

[74] Barros, G.; Lang, M. J.; Mouchtouris, N.; Sharan, A. D.; Wu, C. (2018). Impact of trajectory planning with susceptibility-weighted imaging for intracranial electrode implantation, *Operative Neurosurgery*, Vol. 15, No. 1, 60–65. doi:10.1093/ons/opx215

[75] Minkin, K.; Gabrovski, K.; Penkov, M.; Todorov, Y.; Tanova, R.; Milenova, Y.; Romansky, K.; Dimova, P. (2017). Stereoelectroencephalography Using Magnetic Resonance Angiography for Avascular Trajectory Planning: Technical Report, *NEUROSURGERY*, Vol. 81, No. 4, 688–694. doi:10.1093/neuros/nyx166

[76] Phellan, R.; Forkert, N. D. (2017). Comparison of vessel enhancement algorithms applied to time-of-flight MRA images for cerebrovascular segmentation., *Medical Physics*, Vol. 44, No. 11, 5901–5915. doi:10.1002/mp.12560

[77] Lin, A.; Rawal, S.; Agid, R.; Mandell, D. M. (2018). Cerebrovascular Imaging: Which Test is Best?, *Clinical Neurosurgery*, Vol. 83, No. 1, 5–18. doi:10.1093/neuros/nyx325

[78] Li, K.; Vakharia, V. N.; Sparks, R.; Rodionov, R.; Vos, S. B.; McEvoy, A. W.; Miserocchi, A.; Wang, M.; Ourselin, S.; Duncan, J. S. (2019). Stereoelectroencephalography electrode placement: Detection of blood vessel conflicts., *Epilepsia*. doi:10.1111/epi.16294

[79] Stafa, A.; Leonardi, M. (2008). Role of neuroradiology in evaluating cerebral aneurysms, *Interventional Neuroradiology*, Vol. 14, No. SUPPL. 1, 23–37. doi:10.1177/15910199080140s106

[80]   Kaufmann, T. J.; Huston, J.; Mandrekar, J. N.; Schleck, C. D.; Thielen, K. R.; Kallmes, D. F. (2007). Complications of diagnostic cerebral angiography: evaluation of 19,826 consecutive patients., *Radiology*, Vol. 243, No. 3, 812–9. doi:10.1148/radiol.2433060536

[81]   Vakharia, V. N.; Sparks, R.; Vos, S. B.; McEvoy, A. W.; Miserocchi, A.; Ourselin, S.; Duncan, J. S. (2019). The Effect of Vascular Segmentation Methods on Stereotactic Trajectory Planning for Drug-Resistant Focal Epilepsy: A Retrospective Cohort Study, *World Neurosurgery: X*, Vol. 4, 100057. doi:10.1016/j.wnsx.2019.100057

[82]   Schmidt, R. F.; Lang, M. J.; Hoelscher, C. M.; Jabbour, P. M.; Tjoumakaris, S. I.; Sharan, A. D.; Wu, C. (2018). Flat-Detector Computed Tomography for Evaluation of Intracerebral Vasculature for Planning of Stereoelectroencephalography Electrode Implantation, *World Neurosurgery*, Vol. 110, e585–e592. doi:10.1016/j.wneu.2017.11.063

[83]   Youngerman, B. E.; Khan, F. A.; McKhann, G. M. (2019). Stereoelectroencephalography in epilepsy, cognitive neurophysiology, and psychiatric disease: safety, efficacy, and place in therapy, *NEUROPSYCHIATRIC DISEASE AND TREATMENT*, Vol. 15, No. 1, 1701–1716. doi:10.2147/NDT.S177804

[84]   Yang, M.; Ma, Y.; Li, W.; Shi, X.; Hou, Z.; An, N.; Zhang, C.; Liu, L.; Yang, H.; Zhang, D.; Liu, S. (2017). A Retrospective Analysis of Stereoelectroencephalography and Subdural Electroencephalography for Preoperative Evaluation of Intractable Epilepsy, *Stereotactic and Functional Neurosurgery*, Vol. 95, No. 1, 13–20. doi:10.1159/000453275

[85]   Schauer, D. A.; Linton, O. W. (2009). NCRP Report No. 160, ionizing radiation exposure of the population of the United States, medical exposure - Are we doing less with more, and is there a role for health physicists?, *Health Physics*, Vol. 97, No. 1, 1–5. doi:10.1097/01.HP.0000356672.44380.b7

[86]   Huda, W.; Ogden, K. M.; Khorasani, M. R. (2008). Converting dose-length product to effective dose at CT, *Radiology*, Vol. 248, No. 3, 995–1003. doi:10.1148/radiol.2483071964

[87] Gonzalez-Martinez, J.; Vadera, S.; Mullin, J. P.; Enatsu, R.; Alexopoulos, A. V; Patwardhan, R.; Bingaman, W.; Najm, I. (2014). Robot-assisted stereotactic laser ablation in medically intractable epilepsy: operative technique., *Neurosurgery*, Vol. 10 Suppl 2, 167–72; discussion 172-3. doi:10.1227/NEU.0000000000000286

[88] Mattes, D.; Haynor, D. R.; Vesselle, H.; Lewellen, T. K.; Eubank, W. (2003). PET-CT image registration in the chest using free-form deformations, *IEEE Transactions on Medical Imaging*, Vol. 22, No. 1, 120–128. doi:10.1109/TMI.2003.809072

[89] Vakharia, V. N.; Sparks, R.; O'Keeffe, A. G.; Rodionov, R.; Miserocchi, A.; Mcevoy, A.; Ourselin, S.; Duncan, J. (2017). Accuracy of intracranial electrode placement for stereoencephalography: A systematic review and meta-analysis, *Epilepsia*, No. March. doi:10.1111/epi.13713

[90] Ollivier, I.; Behr, C.; Cebula, H.; Timofeev, A.; Benmekhbi, M.; Valenti, M. P.; Staack, A. M.; Scholly, J.; Kehrli, P.; Hirsch, E.; Proust, F. (2017). Efficacy and safety in frameless robot-assisted stereo-electroencephalography (SEEG) for drug-resistant epilepsy, *NEUROCHIRURGIE*, Vol. 63, No. 4, 286–290. doi:10.1016/j.neuchi.2017.03.002

[91] Bériault, S.; Sadikot, A. F.; Alsubaie, F.; Drouin, S.; Collins, D. L.; Pike, G. B. (2014). Neuronavigation using susceptibility-weighted venography: Application to deep brain stimulation and comparison with gadolinium contrast: Technical note, *Journal of Neurosurgery*, Vol. 121, No. 1, 131–141. doi:10.3171/2014.3.JNS131860

[92] Fifi, J. T.; Meyers, P. M.; Lavine, S. D.; Cox, V.; Silverberg, L.; Mangla, S.; Pile-Spellman, J. (2009). Complications of modern diagnostic cerebral angiography in an academic medical center., *Journal of Vascular and Interventional Radiology : JVIR*, Vol. 20, No. 4, 442–7. doi:10.1016/j.jvir.2009.01.012

[93] Shen, J.; Karki, M.; Jiang, T.; Zhao, B. (2018). Complications associated with diagnostic cerebral angiography: A retrospective analysis of 644 consecutive cerebral angiographic cases., *Neurology India*, Vol. 66, No. 4, 1154–

1158. doi:10.4103/0028-3886.237018

[94] McGovern, R. A.; Butler, R. S.; Bena, J.; Gonzalez-Martinez, J. (2019). Incorporating New Technology Into a Surgical Technique: The Learning Curve of a Single Surgeon's Stereo-Electroencephalography Experience, *Neurosurgery*, Vol. 0, No. 0, 1–2. doi:10.1093/neuros/nyz498

[95] Cardinale, F. (2020). Commentary: Incorporating New Technology Into a Surgical Technique: The Learning Curve of a Single Surgeon's Stereo-Electroencephalography Experience., *Neurosurgery*, Vol. 86, No. 3, E290–E291. doi:10.1093/neuros/nyz569

[96] Manninen, A. L.; Isokangas, J. M.; Karttunen, A.; Siniluoto, T.; Nieminen, M. T. (2012). A comparison of radiation exposure between diagnostic CTA and DSA examinations of cerebral and cervicocerebral vessels, *American Journal of Neuroradiology*, Vol. 33, No. 11, 2038–2042. doi:10.3174/ajnr.A3123

[97] Yi, H. J.; Sung, J. H.; Lee, D. H.; Kim, S. W.; Lee, S. W. (2017). Analysis of Radiation Doses and Dose Reduction Strategies During Cerebral Digital Subtraction Angiography, *World Neurosurgery*, Vol. 100, 216–223. doi:10.1016/j.wneu.2017.01.004

[98] Isoardi, P.; D'Ercole, L.; Cavallari, M.; Gianusso, L.; Pini, S.; Giordano, C.; Angelini, L.; Colombo, P. E.; Canne, S. D.; Vecchio, A. Del; Di Liberto, R.; Farnedi, S.; Ghetti, C.; Lorenzini, E.; Origgi, D.; Paruccini, N.; Pasquino, M.; Cutaia, C.; Quattrocchi, M.; Riccardi, L.; Soavi, R.; Strocchi, S.; Trianni, A.; Venturi, G. (2019). Patient dose in angiographic interventional procedures: A multicentre study in Italy, *Physica Medica*, Vol. 64, No. June, 273–292. doi:10.1016/j.ejmp.2019.06.008

[99] Vakharia, V. N.; Sparks, R.; Rodionov, R.; Vos, S. B.; Dorfer, C.; Miller, J.; Nilsson, D.; Tisdall, M.; Wolfsberger, S.; McEvoy, A. W.; Miserocchi, A.; Winston, G. P.; O'Keeffe, A. G.; Ourselin, S.; Duncan, J. S. (2018). Computer-assisted planning for the insertion of stereoelectroencephalography electrodes for the investigation of drug-resistant focal epilepsy: an external validation study, *Journal of*

Neurosurgery, Vol. 130, No. 2, 601–610. doi:10.3171/2017.10.jns171826

[100] De Momi, E.; Caborni, C.; Cardinale, F.; Castana, L.; Casaceli, G.; Cossu, M.; Antiga, L.; Ferrigno, G. (2013). Automatic trajectory planner for StereoElectroEncephaloGraphy procedures: A retrospective study, *IEEE Trans Biomed Eng*, Vol. 60, No. 4, 986–993. doi:10.1109/TBME.2012.2231681

[101] Kunieda, T.; Kikuchi, T.; Miyamoto, S. (2012). Epilepsy surgery: surgical aspects., *Current Opinion in Anaesthesiology*, Vol. 25, No. 5, 533–9. doi:10.1097/ACO.0b013e32835774d4

[102] Alomar, S.; Jones, J.; Maldonado, A.; Gonzalez-Martinez, J. (2016). The Stereo-Electroencephalography Methodology, *Neurosurgery Clinics of North America*, Vol. 27, No. 1, 83–95. doi:10.1016/j.nec.2015.08.003

[103] Cardinale, F.; González-Martínez, J.; Lo Russo, G. (2016). SEEG, Happy Anniversary!, *World Neurosurgery*, Vol. 85, 1–2. doi:10.1016/j.wneu.2015.11.029

[104] Isnard, J.; Taussig, D.; Bartolomei, F.; Bourdillon, P.; Catenoix, H.; Chassoux, F.; Chipaux, M.; Clémenceau, S.; Colnat-Coulbois, S.; Denuelle, M.; Derrey, S.; Devaux, B.; Dorfmüller, G.; Gilard, V.; Guenot, M.; Job-Chapron, A. S.; Landré, E.; Lebas, A.; Maillard, L.; McGonigal, A.; Minotti, L.; Montavont, A.; Navarro, V.; Nica, A.; Reyns, N.; Scholly, J.; Sol, J. C.; Szurhaj, W.; Trebuchon, A.; Tyvaert, L.; Valenti-Hirsch, M. P.; Valton, L.; Vignal, J. P.; Sauleau, P. (2018). French guidelines on stereoelectroencephalography (SEEG), *Neurophysiologie Clinique*, Vol. 48, No. 1, 5–13. doi:10.1016/j.neucli.2017.11.005

[105] De Momi, E.; Caborni, C.; Cardinale, F.; Casaceli, G.; Castana, L.; Cossu, M.; Mai, R.; Gozzo, F.; Francione, S.; Tassi, L.; Lo Russo, G.; Antiga, L.; Ferrigno, G. (2014). Multi-trajectories automatic planner for StereoElectroEncephaloGraphy (SEEG), *International Journal of Computer Assisted Radiology and Surgery*, Vol. 9, No. 6, 1087–1097. doi:10.1007/s11548-014-1004-1

[106] Nowell, M.; Rodionov, R.; Zombori, G.; Sparks, R.; Winston,

G.; Kinghorn, J.; Diehl, B.; Wehner, T.; Miserocchi, A.; McEvoy, A. W.; Ourselin, S.; Duncan, J. (2015). Utility of 3D multimodality imaging in the implantation of intracranial electrodes in epilepsy, *Epilepsia*, Vol. 56, No. 3, 403–413. doi:10.1111/epi.12924

[107] Sansur, C. A.; Frysinger, R. C.; Pouratian, N.; Fu, K. M.; Bittl, M.; Oskouian, R. J.; Laws, E. R.; Elias, W. J. (2007). Incidence of symptomatic hemorrhage after stereotactic electrode placement, *Journal of Neurosurgery*, Vol. 107, No. 5, 998–1003. doi:10.3171/JNS-07/11/0998

[108] Scorza, D.; De Momi, E.; Plaino, L.; Amoroso, G.; Arnulfo, G.; Narizzano, M.; Kabongo, L.; Cardinale, F. (2017). Retrospective evaluation and SEEG trajectory analysis for interactive multi-trajectory planner assistant, *International Journal of Computer Assisted Radiology and Surgery*, Vol. 12, No. 10, 1727–1738. doi:10.1007/s11548-017-1641-2

[109] Zhao, Y.; Essert, C.; Dergachyova, O.; Haegelen, C.; Jannin, P. (2018). Automatic preoperative planning of DBS electrode placement using anatomo-clinical atlases and volume of tissue activated, *International Journal of Computer Assisted Radiology and Surgery*, Vol. 13, No. 7, 1117–1128. doi:10.1007/s11548-018-1724-8

[110] Herghelegiu, P. C.; Manta, V.; Perin, R.; Bruckner, S.; Gröller, E. (2012). Biopsy Planner - Visual Analysis for Needle Pathway Planning in Deep Seated Brain Tumor Biopsy, *Computer Graphics Forum*, Vol. 31, No. 3pt2, 1085–1094. doi:10.1111/j.1467-8659.2012.03101.x

[111] Belbachir, E.; Golkar, E.; Bayle, B.; Essert, C. (2018). Automatic planning of needle placement for robot-assisted percutaneous procedures, *International Journal of Computer Assisted Radiology and Surgery*, Vol. 13, No. 9, 1429–1438. doi:10.1007/s11548-018-1754-2

[112] Rincon-Nigro, M.; Navkar, N. V.; Tsekos, N. V.; Deng, Z. (2014). GPU-accelerated interactive visualization and planning of neurosurgical interventions, *IEEE Computer Graphics and Applications*, Vol. 34, No. 1, 22–31. doi:10.1109/MCG.2013.35

[113] Trope, M.; Shamir, R. R.; Joskowicz, L.; Medress, Z.;

Rosenthal, G.; Mayer, A.; Levin, N.; Bick, A.; Shoshan, Y. (2014). The role of automatic computer-aided surgical trajectory planning in improving the expected safety of stereotactic neurosurgery, *International Journal of Computer Assisted Radiology and Surgery*, Vol. 10, No. 7, 1127–1140. doi:10.1007/s11548-014-1126-5

[114] Sparks, R.; Zombori, G.; Rodionov, R.; Nowell, M.; Vos, S. B.; Zuluaga, M. A.; Diehl, B.; Wehner, T.; Miserocchi, A.; McEvoy, A. W.; Duncan, J. S.; Ourselin, S. (2017). Automated multiple trajectory planning algorithm for the placement of stereo-electroencephalography (SEEG) electrodes in epilepsy treatment, *International Journal of Computer Assisted Radiology and Surgery*, Vol. 12, No. 1, 123–136. doi:10.1007/s11548-016-1452-x

[115] Essert, C.; Fernandez-Vidal, S.; Capobianco, A.; Haegelen, C.; Karachi, C.; Bardinet, E.; Marchal, M.; Jannin, P. (2015). Statistical study of parameters for deep brain stimulation automatic preoperative planning of electrodes trajectories, *International Journal of Computer Assisted Radiology and Surgery*, Vol. 10, No. 12, 1973–1983. doi:10.1007/s11548-015-1263-5

[116] De León-Cuevas, A.; Tovar-Arriaga, S.; González-Gutiérrez, A.; Aceves-Fernández, M. A. (2017). Risk map generation for keyhole neurosurgery using fuzzy logic for trajectory evaluation, *Neurocomputing*, Vol. 233, No. August 2016, 81–89. doi:10.1016/j.neucom.2016.08.115

[117] Zelmann, R.; Beriault, S.; Marinho, M. M.; Mok, K.; Hall, J. A.; Guizard, N.; Haegelen, C.; Olivier, A.; Pike, G. B.; Collins, D. L. (2015). Improving recorded volume in mesial temporal lobe by optimizing stereotactic intracranial electrode implantation planning, *International Journal of Computer Assisted Radiology and Surgery*, Vol. 10, No. 10, 1599–1615. doi:10.1007/s11548-015-1165-6

[118] Pastori, C.; Francione, S.; Pelle, F.; de Curtis, M.; Gnatkovsky, V. (2016). Fluency tasks generate beta-gamma activity in language-related cortical areas of patients during stereo-EEG monitoring, *Brain and Language*, Vol. 163, 50–56. doi:10.1016/j.bandl.2016.09.006

[119] Munyon, C.; Sweet, J.; Luders, H.; Lhatoo, S.; Miller, J. (2015). The 3-Dimensional Grid: A Novel Approach to Stereoelectroencephalography, *Operative Neurosurgery*, Vol. 11, No. 1, 127–134. doi:10.1227/NEU.0000000000000649

[120] Higueras-Esteban, A.; Delgado-Martínez, I.; Serrano, L.; Principe, A.; Enriquez, C. P.; González Ballester, M. A.; Rocamora, R.; Conesa, G.; Serra, L. (2021). SYLVIUS: A multimodal and multidisciplinary platform for epilepsy surgery, *Computer Methods and Programs in Biomedicine*, Vol. 203, 106042. doi:https://doi.org/10.1016/j.cmpb.2021.106042

[121] Schroeder, W.; Martin, K.; Lorensen, B. (2006). *The Visualization Toolkit* (4th ed.), Kitware, Inc

[122] Maurer, C. R.; Rensheng Qi; Raghavan, V. (2003). A linear time algorithm for computing exact Euclidean distance transforms of binary images in arbitrary dimensions, *IEEE Transactions on Pattern Analysis and Machine Intelligence*, Vol. 25, No. 2, 265–270. doi:10.1109/TPAMI.2003.1177156

[123] Vakharia, V. N.; Duncan, J. S. (2020). Automation Advances in Stereoelectroencephalography Planning, *Neurosurgery Clinics of North America*, Vol. 31, No. 3, 407–419. doi:10.1016/j.nec.2020.03.005

[124] Delgado-Martínez, I.; Serrano, L.; Higueras-Esteban, A.; Vivas, E.; Rocamora, R.; González Ballester, M. A.; Serra, L.; Conesa, G. (2021). On the Use of Digital Subtraction Angiography in Stereoelectroencephalography Surgical Planning to Prevent Collisions with Vessels, *World Neurosurgery*, Vol. 147, 47–56. doi:10.1016/j.wneu.2020.11.103

[125] Zuluaga, M. A.; Rodionov, R.; Nowell, M.; Achhala, S.; Zombori, G.; Mendelson, A. F.; Cardoso, M. J.; Miserocchi, A.; McEvoy, A. W.; Duncan, J. S.; Ourselin, S. (2015). Stability, structure and scale: improvements in multi-modal vessel extraction for SEEG trajectory planning, *International Journal of Computer Assisted Radiology and Surgery*, Vol. 10, No. 8, 1227–1237. doi:10.1007/s11548-015-1174-5